AD-A156 153 PRESSURE CROSS SPECTRA IN TURBULENT BOUNDARY LAYERS IN WATER(U) MINNESOTA UNIV MINNEAPOLIS DEPT OF AEROSPACE ENGINEERING AND M... N NARAYAN ET AL. 14 FEB 85 1/1

UNCLASSIFIED AEM-85-1-RP N00014-83-K-0145 F/G 20/4 NL

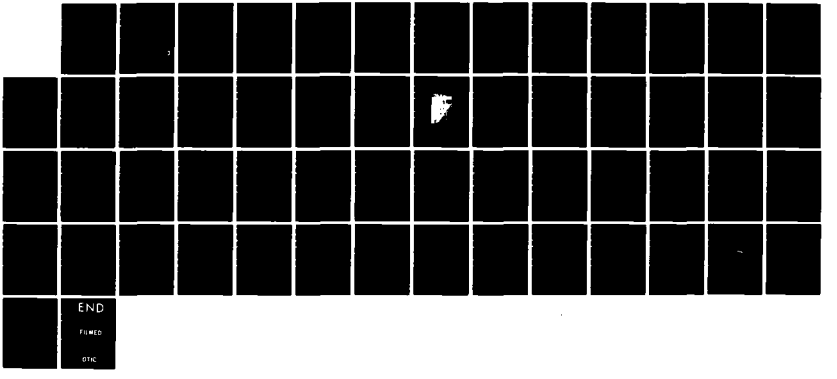

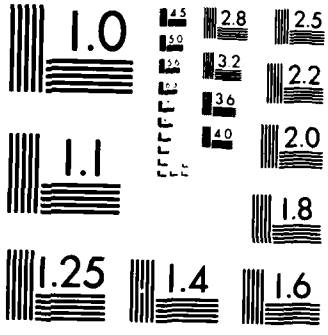

Technical Report TR-AEM-85-1-RP

(2)

Pressure Cross Spectra in Turbulent Boundary Layers in Water

by
Nilabh Narayan, Graduate Student
Robert Plunkett, Professor

Department of Aerospace Engineering and Mechanics
University of Minnesota
Minneapolis, Minnesota, 55455

February 14, 1985

Contract No N00014-83-K-0145 ONR
Dr.M.M.Reischman, Technical Monitor

SECURITY CLASSIFICATION OF THIS PAGE (When Data Entered)

REPORT DOCUMENTATION PAGE

READ INSTRUCTIONS BEFORE COMPLETING FORM

1. REPORT NUMBER: TR-AEM-85-1-RP	2. GOVT ACCESSION NO.
3. RECIPIENT'S CATALOG NUMBER	
4. TITLE (and Subtitle): PRESSURE CROSS SPRECTRA IN TURBULENT BOUNDARY LAYERS IN WATER	5. TYPE OF REPORT & PERIOD COVERED: Interim 6/83 - 12/84
	6. PERFORMING ORG. REPORT NUMBER: TR-AEM-85-1-RP
7. AUTHOR(s): NILABH NARAYAN; ROBERT PLUNKETT	8. CONTRACT OR GRANT NUMBER(s): N00014-83-K-0145
9. PERFORMING ORGANIZATION NAME AND ADDRESS: Dept. of Aerospace Engineering and Mechanics, University of Minnesota, Minneapolis, MN 55455	10. PROGRAM ELEMENT, PROJECT, TASK AREA & WORK UNIT NUMBERS
11. CONTROLLING OFFICE NAME AND ADDRESS: Mechanics Division Code 432, ONR 800 No. Quincy St., Arlington VA 22217	12. REPORT DATE: Feb. 14, 1985
	13. NUMBER OF PAGES: 53
14. MONITORING AGENCY NAME & ADDRESS (if different from Controlling Office)	15. SECURITY CLASS. (of this report): unclassified
	15a. DECLASSIFICATION/DOWNGRADING SCHEDULE

16. DISTRIBUTION STATEMENT (of this Report)

Approved for public release, distribution unlimited

17. DISTRIBUTION STATEMENT (of the abstract entered in Block 20, if different from Report)

18. SUPPLEMENTARY NOTES

19. KEY WORDS (Continue on reverse side if necessary and identify by block number)

Turbulent boundary layer, Hydroacoustics, Cross Spectra, Fluid Solid Interaction

20. ABSTRACT (Continue on reverse side if necessary and identify by block number)

Measurements of the auto and cross spectra of the wall pressure fluctuations in a water tunnel are presented. It is shown that the cross spectra cannot be expressed as a product of functions of the streamwise and transverse coordinates alone but must include interaction terms. One possible parametric approximation is suggested.

DD FORM 1 JAN 73 1473 EDITION OF 1 NOV 65 IS OBSOLETE
S/N 0102-LF-014-6601

SECURITY CLASSIFICATION OF THIS PAGE (When Data Entered)

Introduction

The spectrum (power spectral density) of the vibration level for any linear system can be found by integrating the product of the cross spectrum of the excitation function with the cross frequency response functions of the system over the area on which the excitation is acting. In particular, the spectrum of the vibration response of a plate or shell excited by a turbulent boundary layer is given by [1]:

$$S_{VV}(\mathbf{x}_1,\mathbf{x}_2;\omega)=\int_A\int_A H^*(\mathbf{x}_1,\boldsymbol{\rho}_2;\omega)H(\mathbf{x}_2,\boldsymbol{\rho}_2;\omega)\Gamma(\boldsymbol{\rho}_1,\boldsymbol{\rho}_2;\omega)dA(\boldsymbol{\rho}_1)dA(\boldsymbol{\rho}_2)$$

where $\Gamma(\boldsymbol{\rho}_1,\boldsymbol{\rho}_2,\omega)$ is the cross spectrum of the normal pressure exerted by the boundary layer on the plate,

$H(\mathbf{x},\boldsymbol{\rho},\omega)$ is the response of the plate at $\mathbf{x}$ due to a unit sinusoidal force at $\boldsymbol{\rho}$,

and S_{VV} is the cross spectrum of the response,

Tack and Lambert [2] have demonstrated that this approach accurately predicts the vibration level for a narrow beam exposed to a turbulent boundary layer in a wind tunnel. Most of the papers in the open literature are concerned with ways of approximating H and Γ so as to make the integration relatively simple[3,4] . Our primary objective is to compare the measured response spectrum of a flat plate with that predicted from the measured cross spectra of the pressure field and the measured response functions of the plate. In this way, for at least one case, we will be able to determine what are the controlling variables and what accuracy is necessary in the two cross functions to get acceptable accuracy for the vibration level.

The response functions will be measured for a flat plate in the wall of a water tunnel. In this way we will avoid the calculation of interaction with the water which leads to problems of entrained mass and damping. Since the measurements will be made in place, these effects will already be included in the measurement results. With the same philosophy, the cross spectrum field of the pressure on the wall of the water tunnel was measured directly. In this way we avoid the difficult problem of trying to determine the physical basis for the pressure field in terms of the separate contributions of the incompressible velocity field, the direct radiated acoustic field and the reverberant acoustic field.

This report presents the results of the pressure measurements. Section II describes the water tunnel, the instrumentation and the data reduction system. It also discusses the sensitivity of the instrumentation and the background noise level at the measurement points so that the accuracy and range of validity of the data can be evaluated. Section III presents the measured spectra. Part A presents the autospectrum, shows

that it is almost independent of position in the measurement region, and compares our results with those obtained by others. Part B presents some typical cross spectra and discusses their general characteristics. Section IV discusses appropriate reduced variables for separation distance and frequency and shows a final parametric function fit to all of the data. Section V is a discussion of our results with a comparison with measurements and predictions by others. One important result is that it is impossible to find Γ as a product of functions of x^* and y^* alone since the shape of the transverse cross spectrum changes markedly with axial separation.

Section V is presented here as a matter of peripheral interest since we intend to use only the curve fitted measured spectrum in our final comparison. Other people connected with this project are working on the problem of finding the shape of the cross spectrum, particularly at low wave numbers, with an attempt to simulate the effects of the infinite field for evaluation of theoretical predictions. No such effort has been made by us since we are interested only in the actual response in the finite tunnel used. The detailed data for the spectra measured at the 71 pairs of positions are not given in this report but only a representative sample is presented. All of the data are stored in digital form on floppy disks and are available for further study.

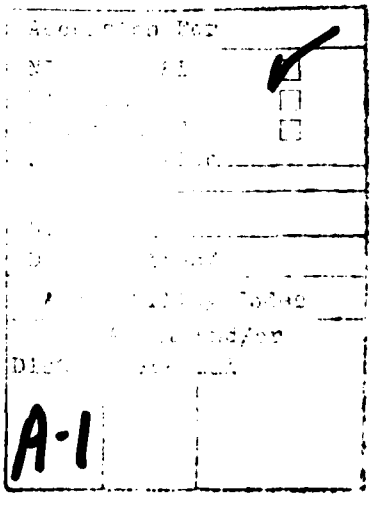

II INSTRUMENTATION

A. Water Tunnel

The measurements were made ir the St. Anthony Falls 7.5 inch square low noise water tunnel [5]. The test section has steel walls with a plexiglas window on one side and is separated from an 18 inch high still water chamber by a thin plexiglas partition (fig. 1). There is a 100 to 1 area reduction from the main stilling chamber to the test section; the upper partition is shaped to the free stream surface so as to create a zero pressure gradient flow. With the partition in place, the static pressure difference between any point in the 1 m long test section and the mean value was less than 3cm of H_2O, or less than 0.5% of the dynamic head at a flow of12.0 m/s.

B. Pressure Transducers

The pressure transducers used were PCB model 105A pressure transducers with a nominal diameter of 2.51 mm and a nominal sensitivity of 2.9 μv/Pa (20 mv/psi). The pressure transducers were held in brass cylindrical holders 38.1 mm in diameter and 12 mm high. The holders were inserted into the partition so that they could be rotated to change the relative positions of the transducers while the faces of the transducers remained flush with the surface. The faces of the holders were sanded to maintain the difference in level to less than 40 μ as the holders were rotated 360°. Two of the holders were placed as close as possible in the transverse direction 800 mm downstream of the tunnel entrance; two others were aligned close together in the downstream direction with the center of one of them 127 mm downstream of one of the first two (fig. 2). Figure 3 is a photograph of this partition with the holders in place. The calculated value of the displacement boundary layer thickness, δ^*, at 12 m/s water velocity is1.6mm at this location and the change in boundary layer thickness is negligibly small in the test region. Later tests showed that the measured pressure autospectrum was the same at all measurement points within ±1dB. By using various combinations of angles, it was possible to position pairs of transducers to measure the cross spectra at combinations of transverse and flow direction separations shown in figure 4. The closest spacing was governed by the diameter of the transducers and casings and was 4.2 mm.

C. Electronics

The transducers are built with MOSFET impedance changers which have an output impedance of 100 Ω. They are powered by a two wire, grounded power supply furnished by the manufacturer. The power lead was about 1 m long and was brought out in a thin polyvinyl tube through pass

through fittings in the top cover of the still water section (figure 3). The brass rod used to turn the holder served as the ground return. The power supplies were battery operated to reduce the electrical noise level which is discussed in the section on measured autospectra.

The output from the power supply was connected to one of the two input channels of a 3582A Hewlett-Packard Spectrum Analyzer. This instrument takes 512 12-bit readings in each channel in each time sample which permits a 128 point cross spectrum linearly covering the chosen frequency range. The frequency span at the maximum sampling rate is 25kHz. Our measurements were made in various ranges from 100 Hz to the upper limit although most of them were made with a 2.5 kHz span. The real and imaginary parts of the spectra were each averaged over a number of time samples; most of them were averaged over 256 samples although some shorter and longer averages were taken for check purposes.

The averaged spectra were then transferred to an HP 86B computer for processing and disk storage. The processing was necessary because the cross spectrum is not directly accessible on the Spectrum Analyzer even though it exists in memory and is used to find the transfer function. The spectra shown later in various forms have been taken directly from the data stored on the discs.

D. Background Noise

Figure 5 compares the measured autospectrum levels with that of two types of background noise. The indicated levels are dB rms ref 1 volt with the transducer sensitivity of 2.9 μv/Pa. The -110 dB level corresponds to 1 Pa/$\sqrt{Hz}$. The lowest curve is that taken with the water tunnel not running and shows the residual combination of electronic noise, truncation error in the A/D converter and the structural vibration in the building. The intermediate curve is one of several taken at 12m/s with the transducer holder hung in the still water section above the partition so that the transducer pointed upstream, downstream or transversely. The highest curve is the measured autospectrum taken with 256 averages; none of the measured autospectra with 256 averages differed from this one by more than ±1dB. All of the cross spectra lay between the top two curves.

Since the partition is acoustically transparent in the frequency range of interest, we interpret the still water spectrum to be that due to the reverberant acoustic field in the water tunnel. This interpretation is bolstered by two rather broad peaks ($Q<3$) at frequencies corresponding to standing halfwavelengths in the vertical and transverse directions. This reverberant field level is everywhere at least 8 dB lower than that

of the measured cross spectra and so no correction was made for it.

Vibration measurements were not taken on the transducer holders but the levels can be estimated. Since the autospectra are not dependent on position, the effective force in any frequency band is the square root of the spectrum level times the effective area. The axial correlation length is of the order of the holder diameter and the transverse one is less so that the effective area is about equal to the product of the diameter and the transverse correlation length. The stiffness of the partition is so low that the natural frequency of the mass on this stiffness is well below the frequency range of interest; as a result, the vibration is mass controlled and the acceleration is about equal to the effective force divided by the mass. With these assumptions, the ratio of the voltage due to acceleration to that due to pressure is:

$$e_a/e_p = (\alpha_a/\alpha_p)\,\lambda_T/\rho h d$$

where

e_a and e_p are the voltages due to acceleration and pressure

α_a and α_p are the corresponding transducer sensitivities

λ_T is the transverse correlation length

ρ is the mass density of the holder

and h and d are the thickness and diameter of the transducer.
The manufacturer reports that the ratio of the sensitivities is about 15Pa/g. If we estimate λ_T to be about 3 mm, let h=12mm, d=38mm and use 8.7 for the specific gravity of brass, we find 0.001 for the voltage ratio. While this computation is far from accurate, it does show that the acceleration induced voltage is small compared with the direct reading due to pressure.

III MEASURED SPECTRA

A. Autospectrum

The autospectra measured at all the available positions of the holders agreed within the 12 bit resolution or ± 1dB. Most of the measurements were taken with a water velocity of 12 m/s. Figure 6 shows the autospectrum for both 4 and 256 averages and a range of 2.5 kHz at this velocity. Figure 7 shows the autospectrum at the same point for 256 averages and a range of 25 kHz with a water velocity of 22m/s. Figure 8 shows the autospectrum for 256 averages and a range of 2.5 kHz at a velocity of 22 m/s. A hanning window which has a noise bandwidth of 30 Hz when the range is 2.5 kHz was used for all measurements. The variance in spectra levels for individual time samples may be estimated from figure 6. Some readings were taken at 2560 averages and these spectra were even smoother than the 256 ave one shown. Above 100 Hz, the dB spectrum level is a linear function of frequency with no local perturbations. Because it is a dB plot, the scatter above the line is less than that below; one would expect the scatter for the 4 average points to be 8 times that for the 256 one which looks about right.

Figure 9 shows a composite plot of the autospectrum level normalised with respect to the dynamic pressure plotted as a function of the frequency normalised with respect to the free stream velocity and the boundary layer thickness. Also shown on the same plot are some measurements previously made by J. Killen using a different type of transducer in the same tunnel. Chase [6] shows that the autospectrum level decreases somewhat for normalised frequencies, $\omega\delta^*/U_c$, less than 0.1 . It appears that the increase we show in spectrum level at frequencies below 100Hz is primarily due to the increased contribution of the reverberant field (figure 5); because of the reduced noise bandwidth, this cutoff frequency is somewhat lower when the measurement is taken with a lower frequency span.

Willmarth [7] shows that the measured pressure increases with decreasing transducer size because the larger diameter transducers integrate out the effect of the short wavelength (high wavenumber) components. However, he shows no further decrease in measured pressure level for $dU_\tau/\upsilon > 100$; we measured the rms pressure to be 540±40Pa at 12m/s which gives a pressure ratio p/q_∞ of 7.3×10^{-3} at a value of $dU_\tau/\upsilon = 1200$ where Willmarth shows 5.5×10^{-3}.

Willmarth [7] reports a ratio p/τ_w of 2.5 with a transducer diameter

ratio $d/\delta^* = 0.33$ and a Reynolds number of 2×10^4. If we let $\tau_W = 1.5 \times 10^{-3} \rho U_\infty$, we get 220 Pa for the wall shear stress which gives us a pressure ratio of 2.45 at a diameter ratio of 1.5 and the same Reynolds number. Willmarth and Woodridge[8] report 2.7 for the shear stress ratio in air at a somewhat higher Reynolds number. Handler et al [9] suggest a ratio of 3.32 derived from a numerical integration of the Navier-Stokes equation at a Reynolds number of 5000.

B. Typical Cross Spectra

The cross spectra were measured for sets of two points covering the separation grid shown in figure 4. The modulus and phase data are available on floppy disks in digital form in HP Basic format for all combinations of transducer separation, frequency spans and numbers of averages shown in Table 1.

This report presents eleven cross spectra typical of different regions of the measurement grid; they include all combinations of 0, 5, 25 and 110mm axial separation and 0, 4 and 8mm transverse separation. Figures 10 and 11 a and b are for 0 axial and 4 and 8mm transverse separation; figures 12,13 and 14 a and b are for 5 mm axial and 0 ,4 and 8 mm transverse separation; figures 15-17 cover 25 mm axial and figures 18-20 cover 110mm axial. The a figures show the modulus of the cross spectrum as dB less than the autospectrum at the same frequency and the b figures show the phase in degrees. Figures 18c,19c and 20c show the modulus for a frequency span of 500 Hz to demonstrate that the low frequency portion of the cross spectrum is almost independent of Δy at at small Δy and large Δx.

The slope of the phase plot multiplied by the axial separation is the phase velocity. A plot of the ratio of this velocity to that of the free stream derived from these and other graphs is shown as a function of frequency with axial separation as a parameter in figure 21. The phase indicated velocity, which we may interpret as being the convected velocity of the turbulence components, decreases with increasing frequency. The values of U_C/U_∞ are about the same as those obtained by Willmarth and Wooldridge in a wind tunnel [8]. The velocity ratio is independent of lateral separation except perhaps at short axial separations where the cross spectrum fell off so rapidly with lateral separation that the phase could not be measured. It can be seen from the phase plots (e.g. Fig 12b) that the slope approaches zero at very low frequency. This indicates that the phase velocity has a maximum at $\omega\delta^*/U_\infty \approx 0.1$ and then drops to 0 at zero frequency. The curve for the shortest separation lies slightly below that of the composite curve at larger Δx.

IV Parametric Fit

The modulus of the cross spectrum falls with frequency at a rate that increases with increasing separation until it reaches a relatively constant level of -13dB relative to the autospectrum. The transition frequency drops from 3.5 kHz at Δx= 5mm, Δy=0 to about 350-400 Hz at Δx=110 mm, Δy= 0,4 or 8mm. The transition frequency for the autospectrum is also about 3.5kHz. At frequencies higher than the transition the variance in the cross spectra among members of the ensemble increases substantially and it also becomes difficult to find a smooth phase curve. This behavior can be seen in figures 13a and b at about 1300 Hz (Δx=5mm), in figures 16a and b at about 1100 Hz (Δx=25mm) and in figures 18a, b and c at about 380 Hz (Δx=110mm). If the number of averages is now greatly increased, the variance in both modulus and phase can be reduced and the phase appears to have an average value of 0^{O} for all frequencies higher than that of the transition region.

Corcos[10] constructed a model of the cross spectrum based on limited data in the axial direction alone and the transverse direction alone. His representation was:

$$\Gamma(x,y,;\omega) = \Gamma_1(0,0;\omega)\Gamma_2(x^*,0)\Gamma_3(0,y^*)$$

where $\Gamma_2 = \exp(-\alpha|x^*|)$ and $\Gamma_3 = \exp(-\beta|y^*|)$

and $x^* = \omega x/U_C$, $y^* = \omega y/U_C$

Figure 22 shows a composite plot of our cross spectrum levels relative to the autospectrum as a function of x^* and y^* and figure 23 shows the same plot from a different viewpoint. Figure 24 shows Γ as a function of x^* with y^*= 0 for Δx=5,10 and 20mm to indicate how well the data are collapsed. Superposing the curves for Δx=15,30,40 and 50mm increases the scatter band little if any. Figure 25 is a similar section for $y^*=0.8x^*$. When Δx=0 the cross spectrum falls off so rapidly with Δy that the finite transducer size makes it impossible to get accurate data. This is no longer as serious a problem at even the shortest flow direction separation of 5.2 mm.

It can be seen that there is a very large interaction between the axial and lateral separation effects so that it is not possible to express Γ in terms of products of functions of x and y separately. Borscherskii et al [11] have analysed the case of an eddy in the process of being ejected from the boundary layer and predict the pressure field by using the Navier-Stokes equations. They find that the decay of the pressure field with distance includes an x^2 term. It is stil convenient to let Γ_2 be a function of x^* alone and let Γ_3 contain the interaction terms. Least squares fits were made for the data points in the pressure dominated

region from all of the cross spectra using various linear and quadratic combinations of x^* and y^*. For $y^*=0$ the appropriate region was $x^*<25$ (fig.24); the upper limit of x^* decreased as Δy increased. For example, $x^*<5$ was used for Δx=5mm and Δy=4mm (fig.25). Points at frequencies below 80 Hz were discarded because the spectrum level was raised by the structural vibrations at low frequencies (fig.5); the corresponding values of x^* are proportional to Δx (fig.24).

For each value of Δx and Δy the normalized cross spectrum was found for each frequency point by subtracting the average of the dB levels of the autospectra at the two corresponding positions. At any frequency, the two autospectra usually agreed within 1 dB, almost always within 2dB and never differed by more than 4 dB. All of the normalized cross spectra for $\Delta y=0$ were used to make a least squares fit with linear and quadratic terms giving:

$$\Gamma_2^{(1)} = \exp(-0.081|x^*| - 0.0010x^{*2})$$

which is the solid curve in figure 24. If only the quadratic term is used:

$$\Gamma_2^{(2)} = \exp(-0.14 - 0.0053x^{*2})$$

which is the dotted curve in figure 24. This shows that at least as good a fit can be had with a purely quadratic term; the 0.6 dB defect at $x^*=0$ (which is the 0.14 term in Γ_2) may be caused by the structural vibration having a slightly greater influence on the autospectrum than it does on the cross spectra.

For each value of Δx the cross spectral values at $\Delta y=0$ were subtracted from each cross spectrum with the same value of Δx. When plotted versus y^* there was considerably more scatter among the curves for different Δy than is shown in figure 24 for Γ_2 versus x^*. A quadratic fir was then made for all of the low frequency data in the pressure controlled region for each value of Δx. The coefficient of y^{*2} was then plotted versus x^*; This reduced data could be fitted with a curve of the form $1/a+b|x^*|$ finally giving:

$$\Gamma_3 = \exp(-5.15y^{*2}/(2.3+|x^*|))$$

Figures 22 and 23 are plots of $\Gamma_2^{(1)}\Gamma_3$ with an arbitrary minimum of -13dB corresponding to the average values at high frequencies in all cross spectra. If there is any change in this value between the transition frequency and 2500 Hz, it is masked by the large fluctuations in the curves. The use of U_c as a scaling factor at large separations and frequencies above the transition region is purely a convenience since the appropriate velocity is the acoustic velocity and not the convected velocity. Such a convention is possible only because the ratio of the convected to acoustic velocities is very small and the wave numbers appropriate to our data are relatively large. This plot clearly cannot be

extrapolated to values of x^* and y^* approaching the reciprocal of the Mach number.

Corcos' curves [10] fit well to:

$$\Gamma_2 = \exp(-0.115|x^*|)$$

and $$\Gamma_3 = \exp(-0.70|y^*|)$$

Corcosused a constant value of 0.6 for U_c/U_∞ instead of letting it vary with ω as was done in this report which accounts for some of the difference between 0.081 and 0.115.

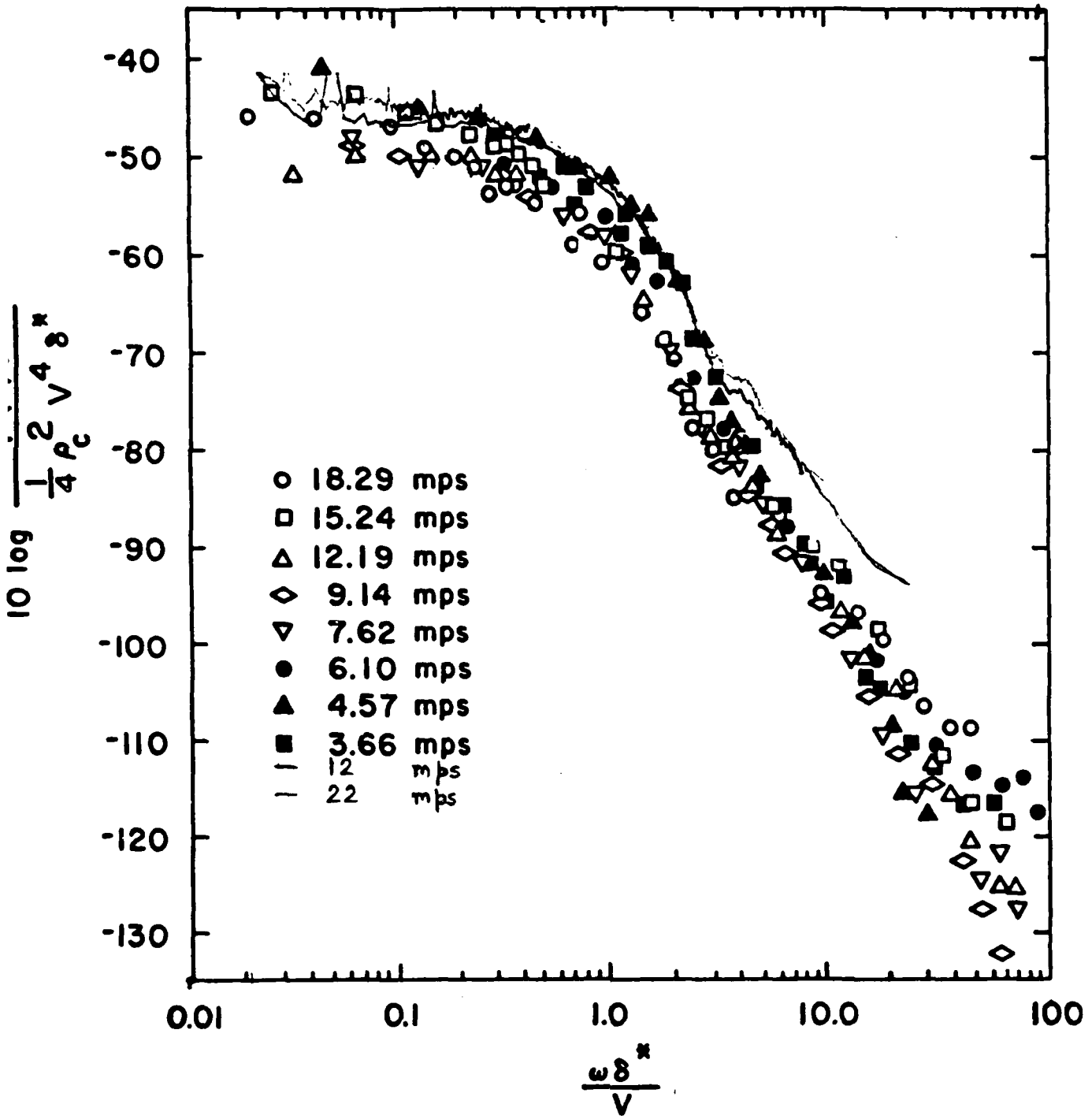
-40
-50
-60
-70
-80
-90
-100
-110
-120
-130
0.01
0.1
1.0
10.0
100
10 log $\frac{\dot{}}{\frac{1}{4}\rho_c^2 V^4 \delta^*}$
$\frac{\omega \delta^*}{V}$
18.29 mps
15.24 mps
12.19 mps
9.14 mps
7.62 mps
6.10 mps
4.57 mps
3.66 mps
12 mps
22 mps

Fig 9

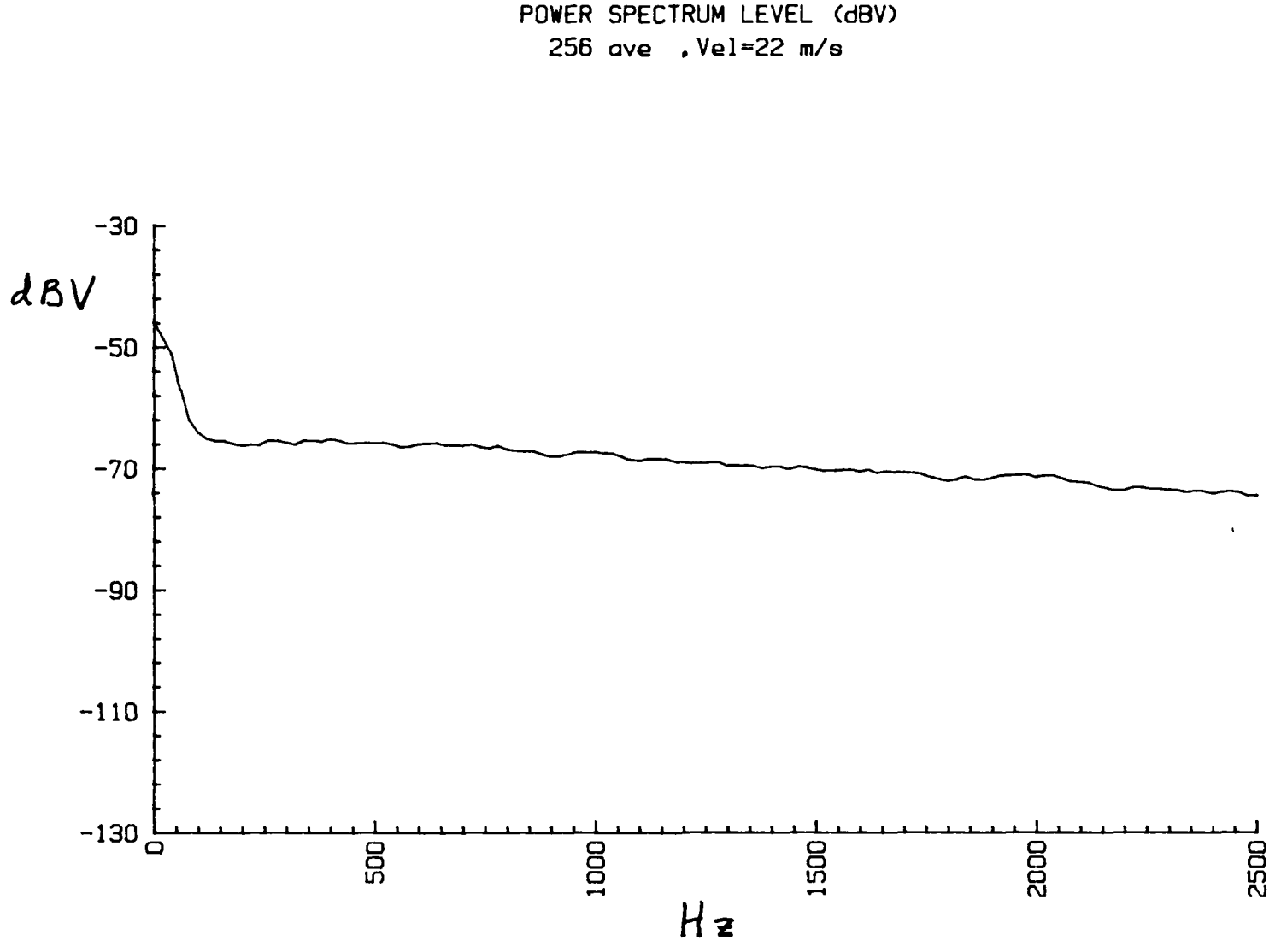
POWER SPECTRUM LEVEL (dBV)
256 ave , Vel=22 m/s
dBV
-30
-50
-70
-90
-110
-130
0
500
1000
1500
2000
2500
Hz

Fig 8

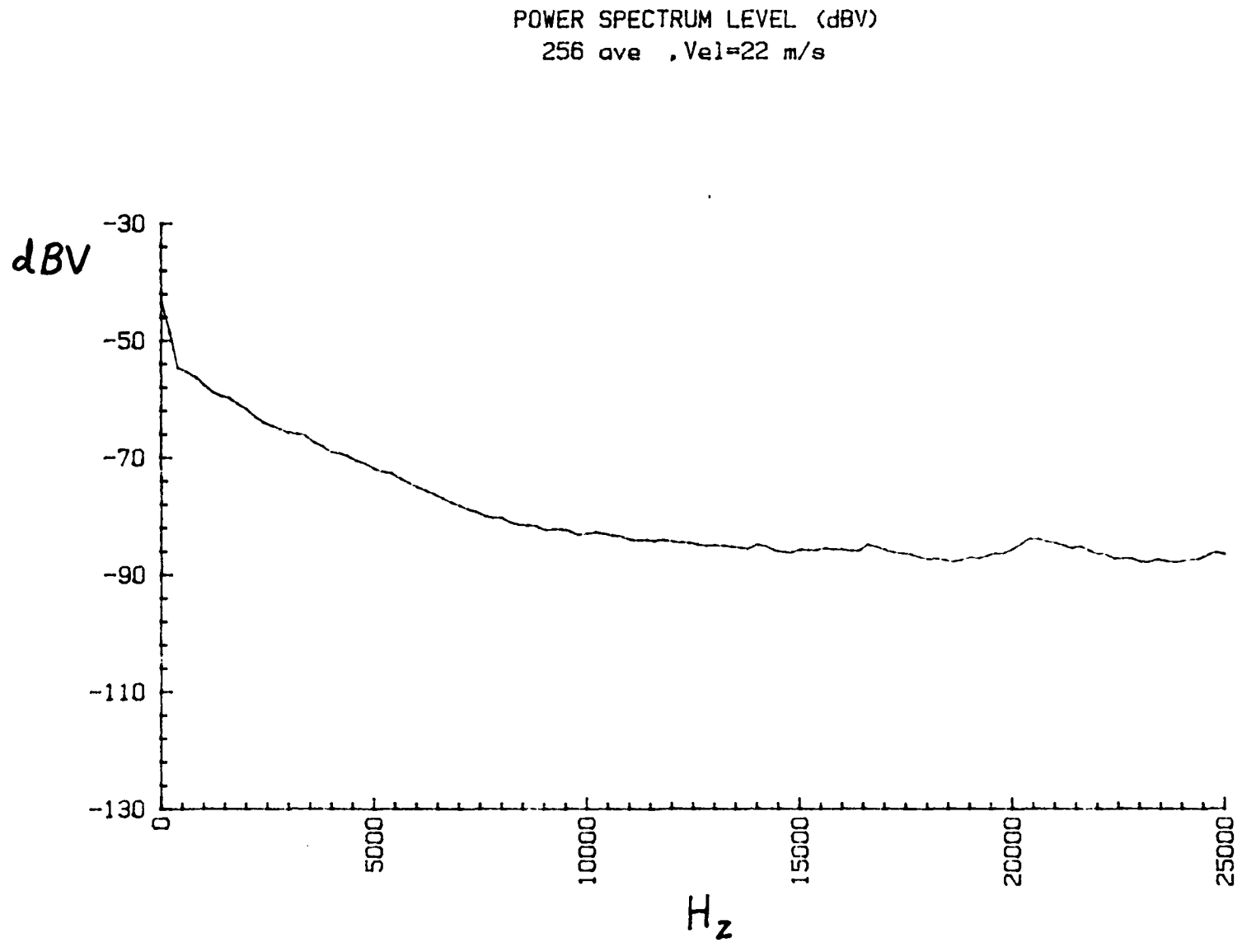
POWER SPECTRUM LEVEL (dBV)
256 ave , Vel=22 m/s
dBV
-30
-50
-70
-90
-110
-130
0
5000
10000
15000
20000
25000
Hz

Fig 7

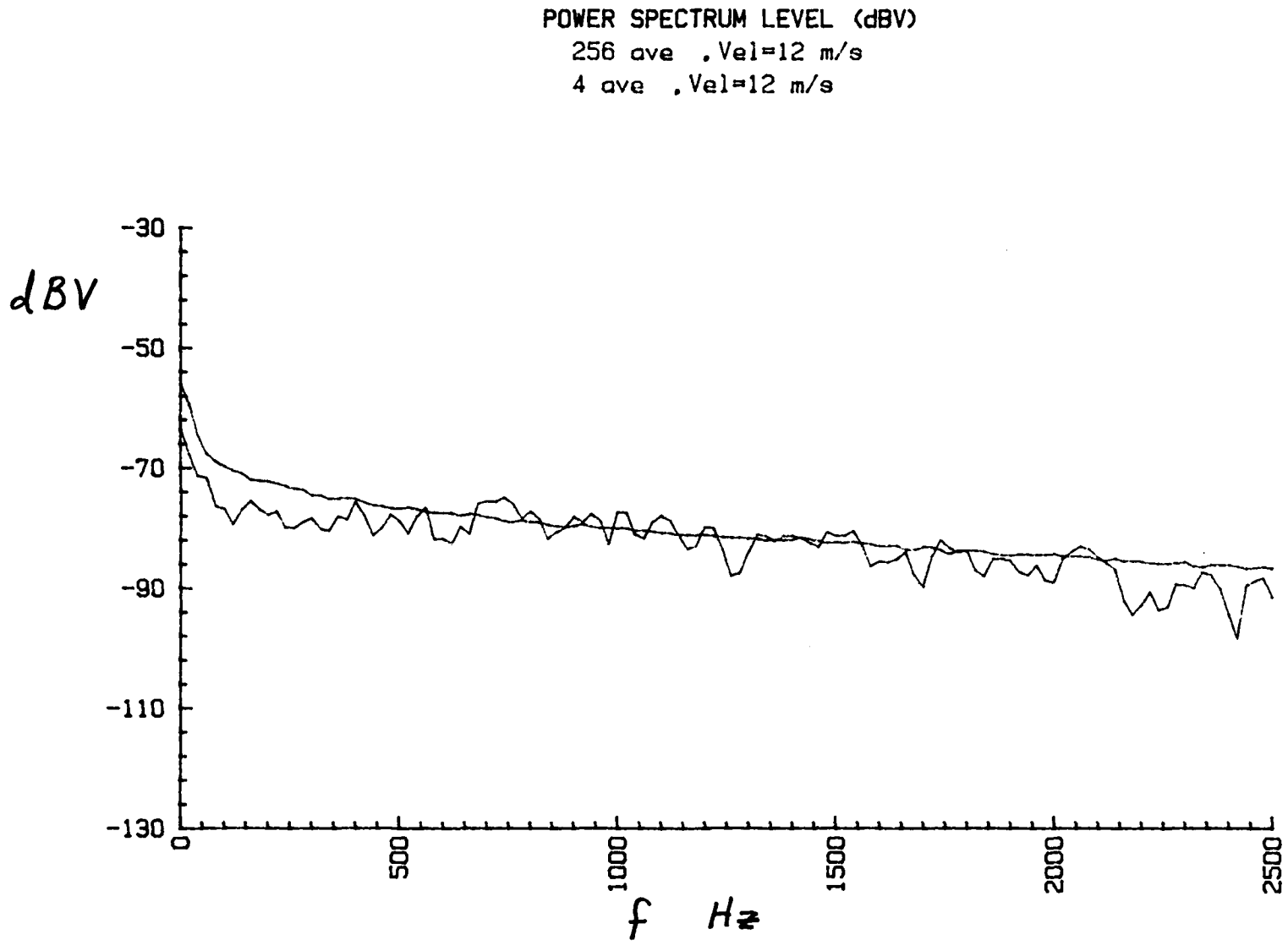
POWER SPECTRUM LEVEL (dBV)
256 ave . Vel=12 m/s
4 ave . Vel=12 m/s
dBV
-30
-50
-70
-90
-110
-130
0
500
1000
1500
2000
2500
f Hz

Fig 6

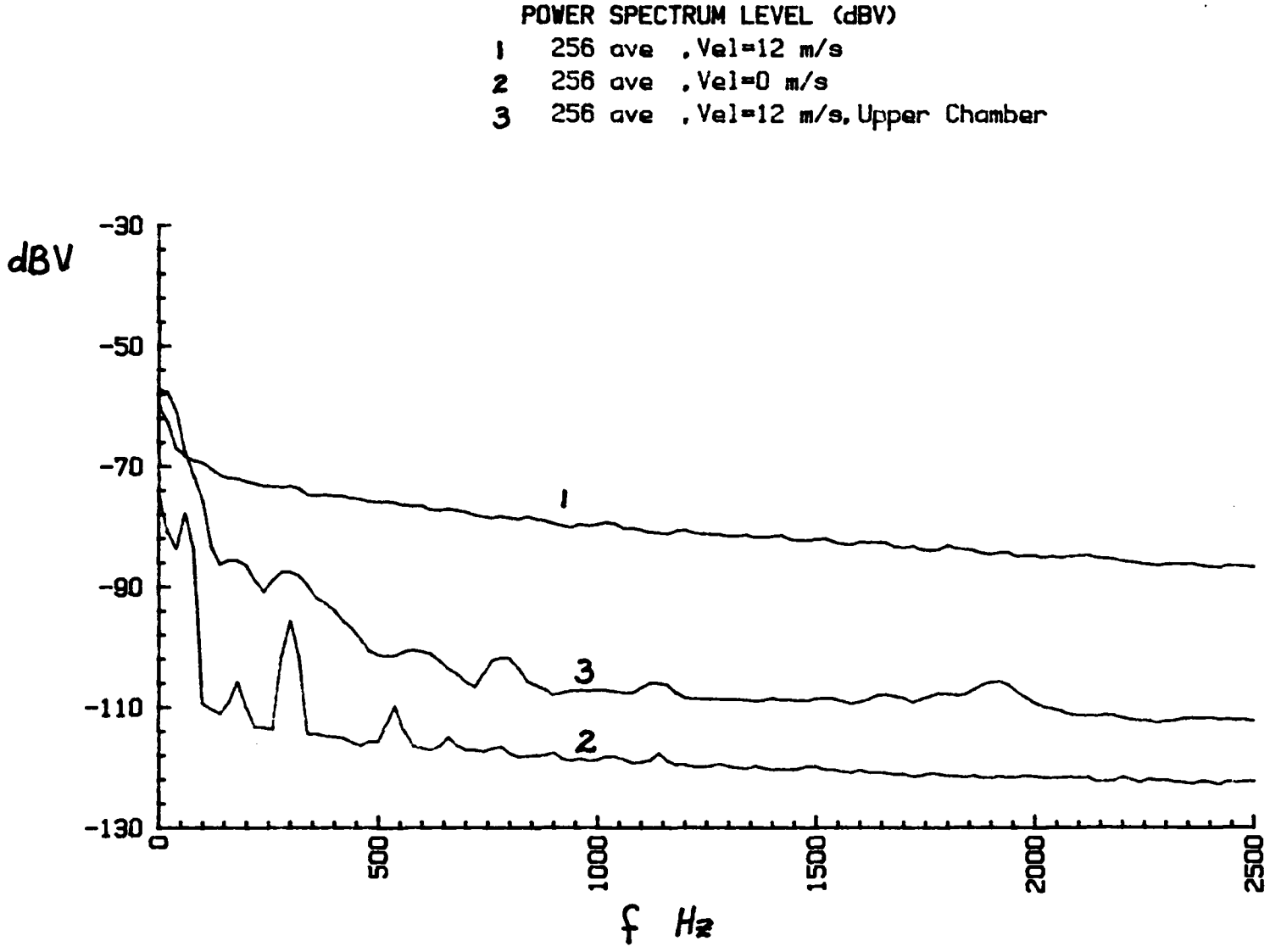
POWER SPECTRUM LEVEL (dBV)
1 256 ave . Vel=12 m/s
2 256 ave . Vel=0 m/s
3 256 ave . Vel=12 m/s, Upper Chamber
dBV
-30
-50
-70
-90
-110
-130
0
500
1000
1500
2000
2500
f Hz
1
2
3

Fig 5

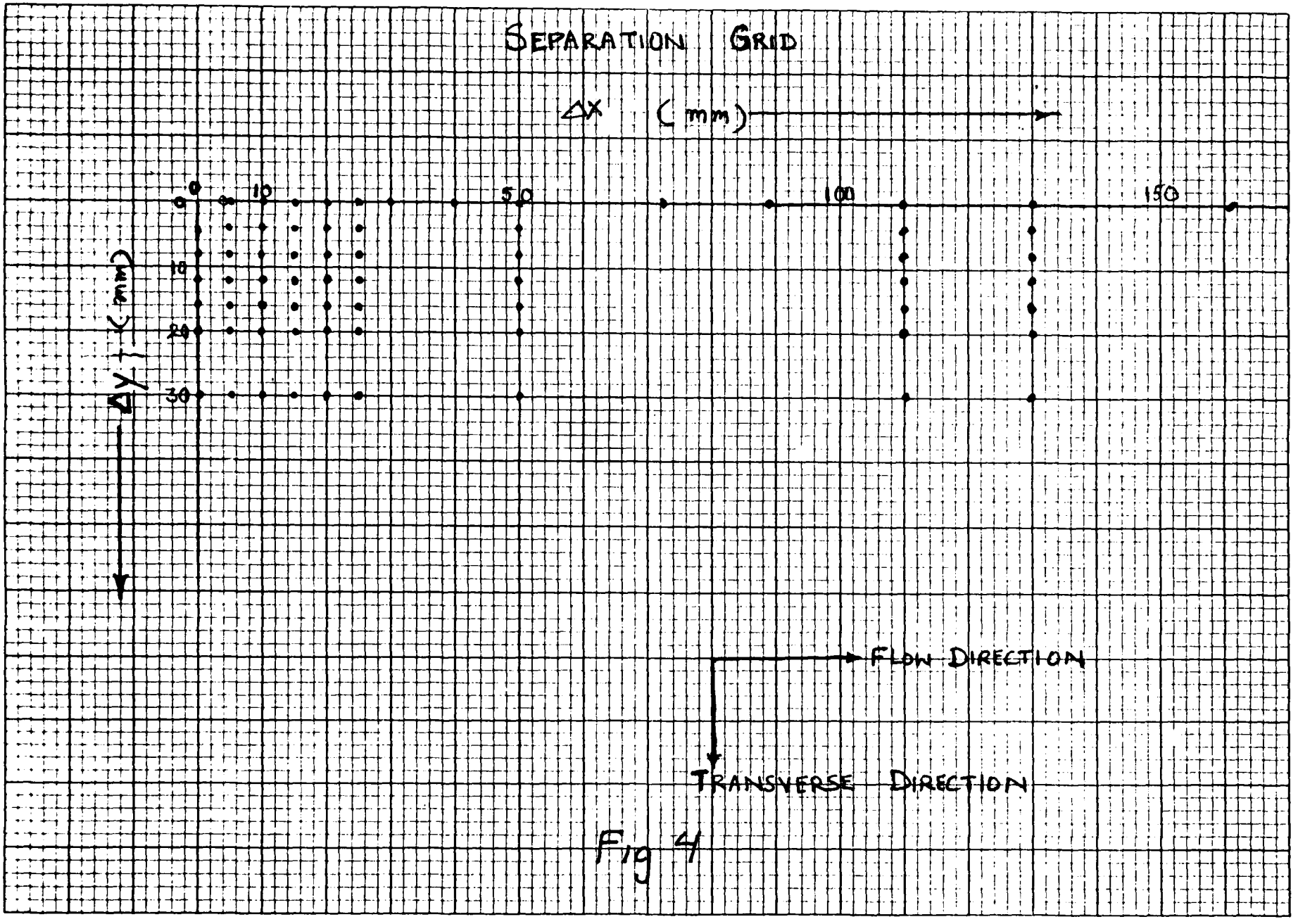
SEPARATION GRID
Δx (mm)
0
10
50
100
150
Δy (mm)
0
10
20
30
FLOW DIRECTION
TRANSVERSE DIRECTION

Fig 4

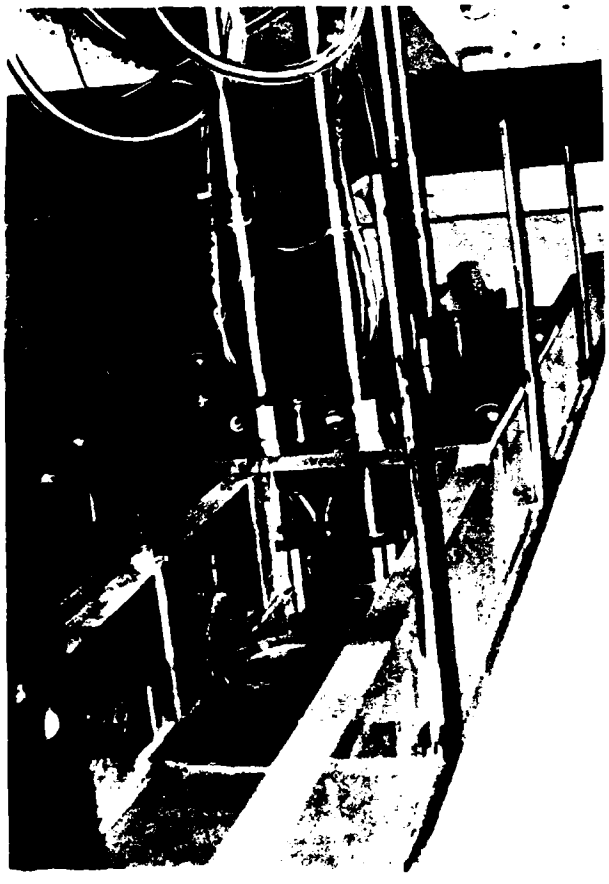

Fig 3

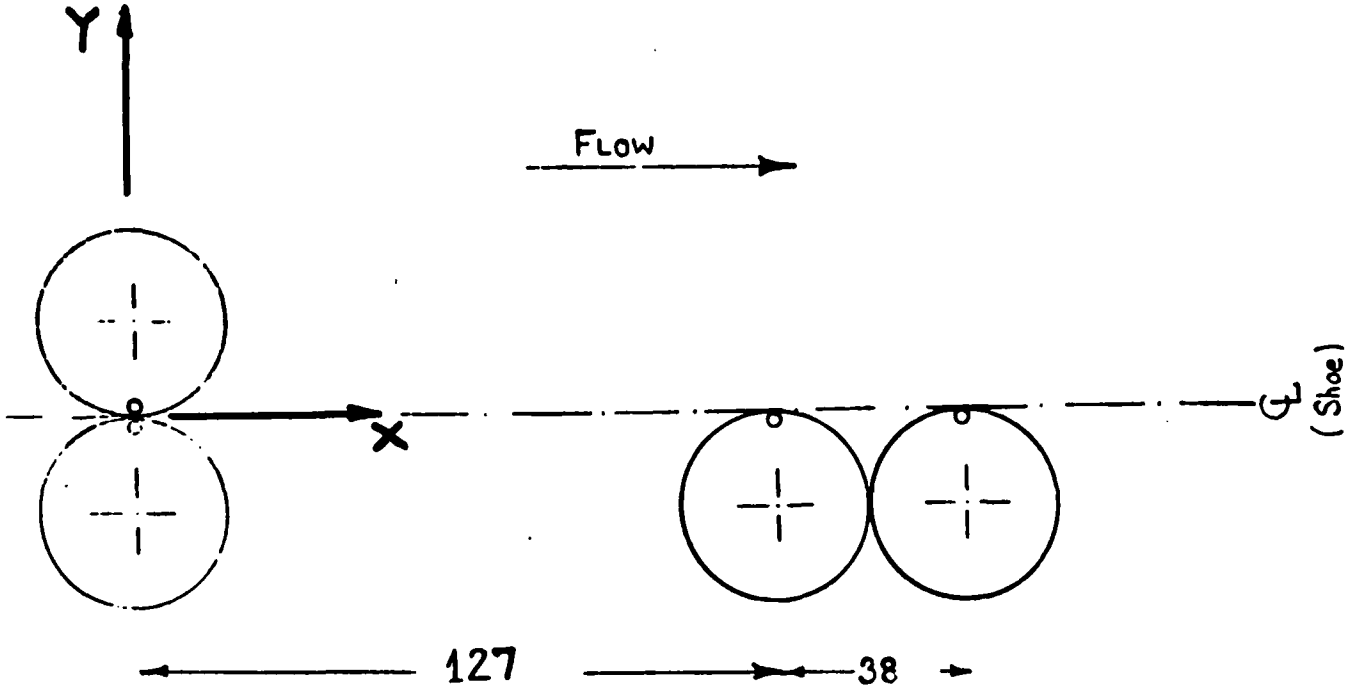

Fig 2 Holder Configuration

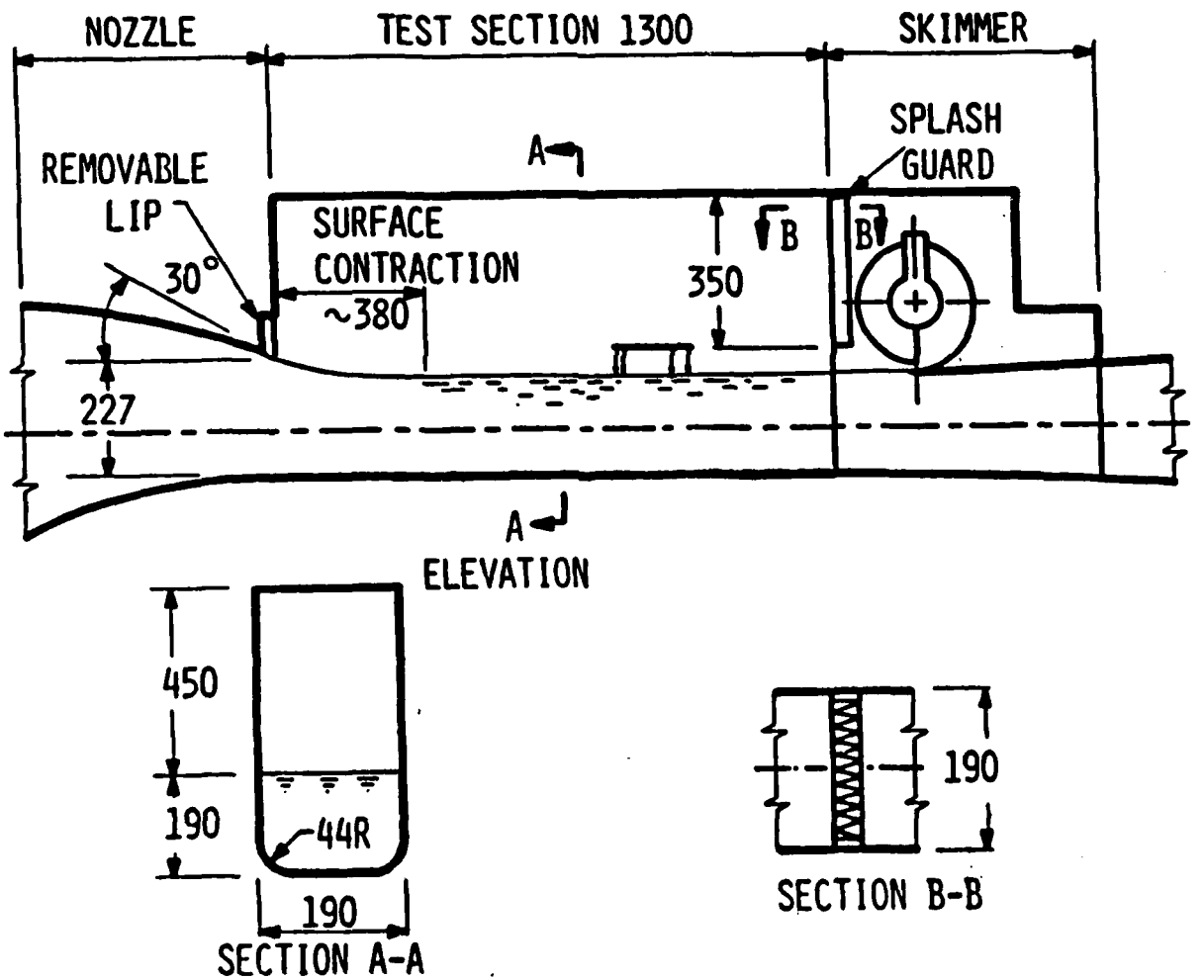

Fig.1 - Test section configuration

Figures

14. Kline, S.J., W.C.Reynolds, F.A.Scraub and P.W.Runstadler, "The Structure of Turbulent Boundary Layers" JFM, 30,4,741-773 (1967)

15. Haddle, G.P. and E.J.Skurdzyk "The Physics of Flow Noise", JASA 46,1(Pt.2),1969, 130-157

References

1. Lin, Y.K. "Probabalistic Theory of Structural Dynamics", McGraw-Hill, 1967, equation 7-14

2. Tack, D.H. and R.F.Lambert "Response of Bars and Plates to Boundary-Layer Turbulence", J.Aerospace Sci., 29, 3, March 1962, 311-322

3. Powell, A. "Response of Structures to Random Pressures" Chap. 8, Random Vibration, S.H.Crandall, ed. ,MIT Press, 1958

4. Chandirimani, K.L. "Vibration Response of Fluid Loaded Structures to Low Speed Flow Noise" JASA, 61, 1977, 1460-1470

5. Wetzel,J. M. and J. M. Killen "The Saint Anthony Falls Hydraulic Laboratory High Speed Varaiable Pressure, Free Surface Flow Facility" Paper prepared for NATO Seminar March 1982, Saint Anthony Falls Hydraulic Laboratory, University of Minnesota, Minneapolis, MN

6. Chase, D.M. "Modeling the Wavevector-Frequency Spectrum of Turbulent Boundary Layer Wall Pressure" J Sound Vib., 70, 1, 29-67, 1980

7. Wilmarth, W.W. "Pressure Fluctuation beneath a Turbulent Boundary Layer" Ann. Rev. Fl. Mech, 7, 1975, 13-38

8. Wilmarth, W.W. and C.E.Wooldridge "Measurements of the Fluctuating Pressure at the Wall beneath a Thick Turbulent Boundary Layer", JFM, 14, 2, 1952, 187-210

9. Handler, R. A., R.J.Hansen, L.Sakell, S.A.Orszag and E.Bullister "Calculations of the Wall Pressure Field in a Turbulent Channel Flow" Phys.of Fluids, 27, 3, March 1984, 579-582

11. Corcos, G.M. "The Structure of the Turbulent Pressure Field in Boundary Layer Flows" JFM 18,3, 1964 , 353-378

12. Borshcherskii, Yu.T., E.M. Litvinenko and V.G. Nakharchuk, "Kinematics of Turbulent Boundary Layers ", Fluid Dynamics, 8,5,1973,707-712 (translation from Mekhanika Zhidkoskii i Gaza 8,5,1973 34-40)

13. Ffowcs-Williams, J.E. "Boundary-Layer Pressure and the Corcos Model- A Development to Incorporate Low Wavenumber Constraints", JFM, 125, 9-25 (1982)

necessarily much larger than that of the convected field and so it takes many more averages to get a smooth curve. In addition, the variance for the phase (0^0) is larger than that for the modulus.

Willmarth [6] shows that the finite size of the transducer can underestimate the total pressure because of the influence of the high frequency, short wavelength eddies. In figure 5 of his paper he shows that the ratio p/q_∞ decreases monotonically with increasing dimensionless diameter dU_τ/υ up to values of about 50. We get 7.3×10^{-3} for p/q_∞ at a dimensionless diameter of 1260 which is about 40% higher than his reported values. On the other hand, we get exactly the same value of p/τ_w as he reports.

Our primary interest is in finding values for the cross spectrum to use in the integral for finding the response function. We may consider that the transducer has integrated the pressure field over its effective area as indicated by Corcos. This will have no influence on the final integration so long as the response function H does not change much in a distance equal to the diameter of the transducer. Thus, this under estimation of the total rms pressure should not affect the prediction of the vibration response except for modes with wavelengths equal to or less than the diameter of the transducer.

V DISCUSSION

While it is not the purpose of these experiments to explore the microphysics of the turbulent boundary layer, a few comments on the relationship of our results to the measurements, analyses and predictions of others seems in order. Corcos' model is based on the incompressible pressure field [10]. Using this model he demonstrates that the bulk of the pressure energy is generated in the mixing sublayer with the peak at $x_2/\delta^* \approx 0.2$. Ffowcs-Williams [12] has included the compressibility effects in the same model and predicts the importance of a radiated acoustic field at higher frequencies. In a series of articles based on measurements at very low Reynolds numbers and very thick boundary layers, Kline et al. [13] discuss the importance of a streak like structure in the boundary sublayer leading to liftup and ejection from the boundary layer. Haddle and Skurdzyk [14] discuss measurements of the autospectrum in water. They find two frequency regions: a near field velocity dominated region at low frequencies and a far field acoustic region at high frequencies. They note that in water at velocities of 10 to 20 m/s a transducer size of order 0.1 mm would be necessary to resolve Kline streaks. They conclude that the larger, ejected turbulent eddies are the important source of the TBL noise as measured in water by available transducers.

With these previous results in mind, we interpret our measurements to indicate an eddy produced velocity field being convected downstream with a velocity that increases with increasing size and thus lower associated frequency. These eddies waver back and forth as they procede downstream and so the cross spectrum broadens with increasing downstream distance. The smaller eddies and perhaps even the Kline streaks account for a large share of the total energy and so the lateral correlation length is very short at zero axial distance. The increase in lateral correlation length in the downstream direction is accompanied by an increase in the variance from sample to sample. This is indicated by the increased number of averages that is necessary to get smooth data as Δy increases.

As indicated by Ffowcs-Williams, the combination of the velocity induced pressure field and the zero velocity normal boundary condition at the wall gives rise to a radiated pressure field. Since this is caused by radiation from all directions on the surface of an infinite plate, the expectation of the phase must be zero and the cross correlation is essentially independent of distance so long as the separation is small with respect to the velocity of sound divided by the frequency, i.e. the acoustic wavelength. The variance of these acoustic samples is

NORMALIZED CROSS SPECTRUM LEVEL (dB)

256 ave. X =0 mm, Y=4.2 mm, VEL=12 m/s

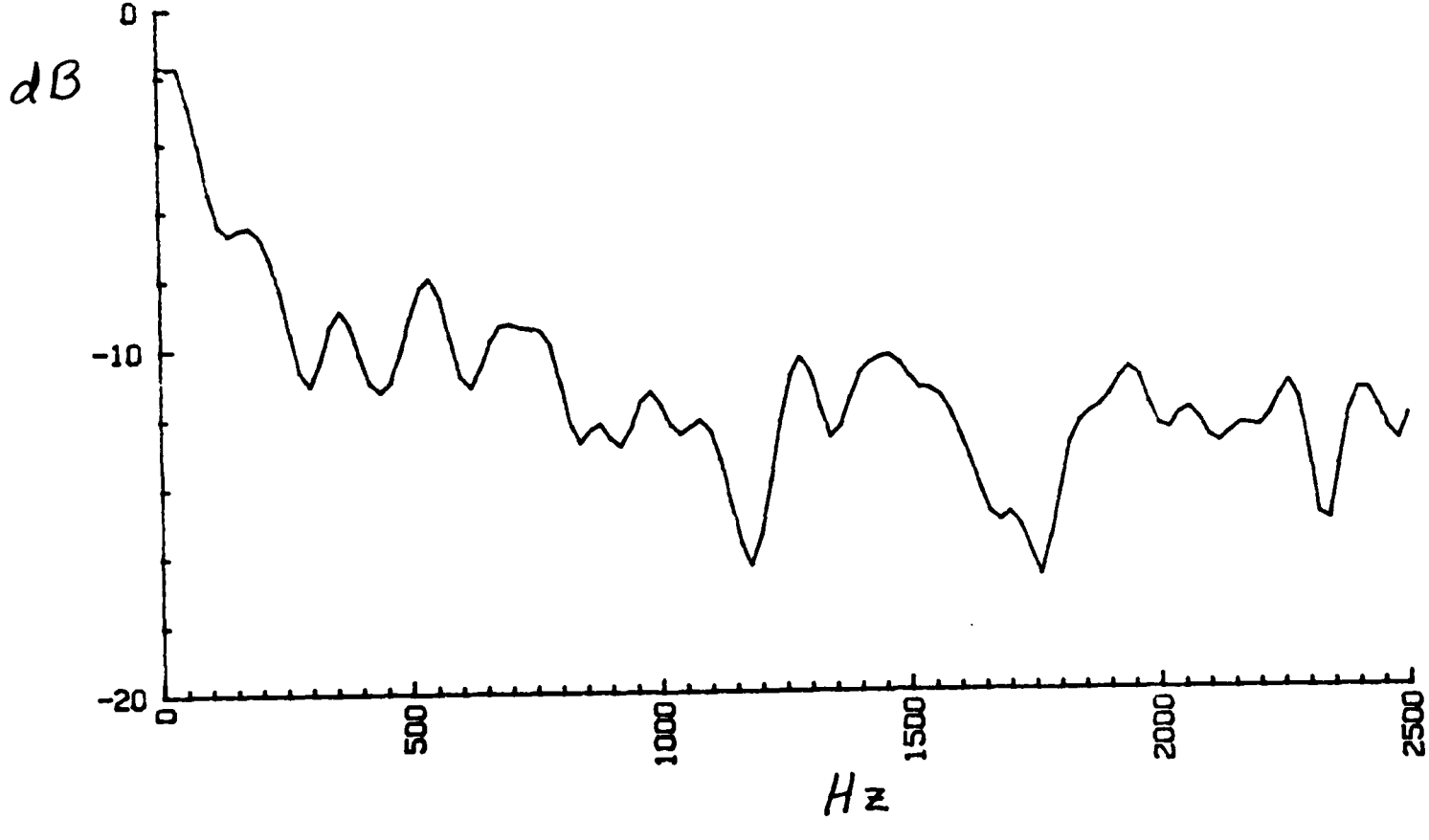

Fig 10a

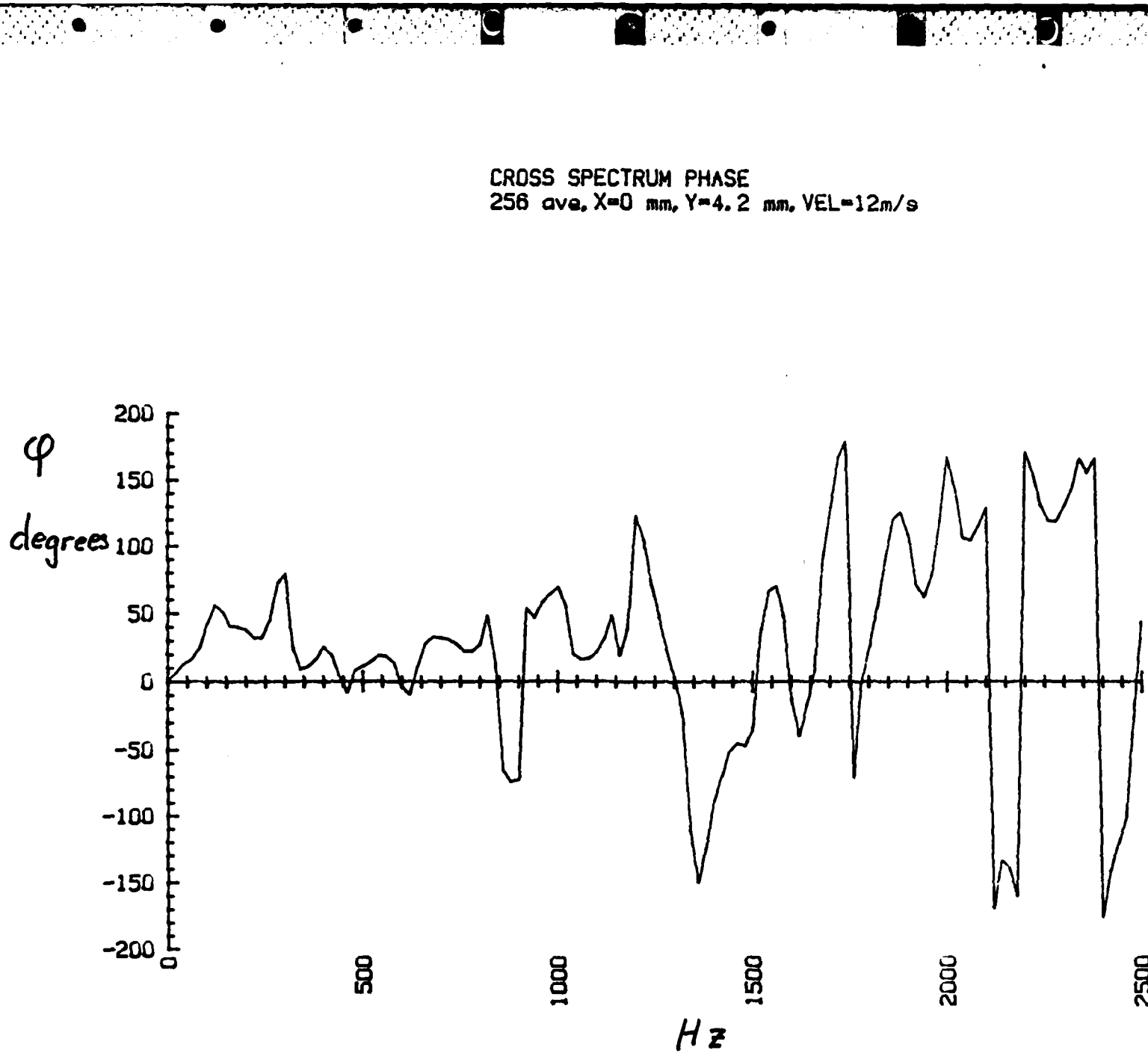
CROSS SPECTRUM PHASE
256 ave. X=0 mm. Y=4.2 mm. VEL=12m/s
φ
degrees
200
150
100
50
0
-50
-100
-150
-200
0
500
1000
1500
2000
2500
Hz

Fig 10b

NORMALIZED CROSS SPECTRUM LEVEL (dB)

256 ave. X =0 mm, Y=8.3 mm, VEL=12 m/s

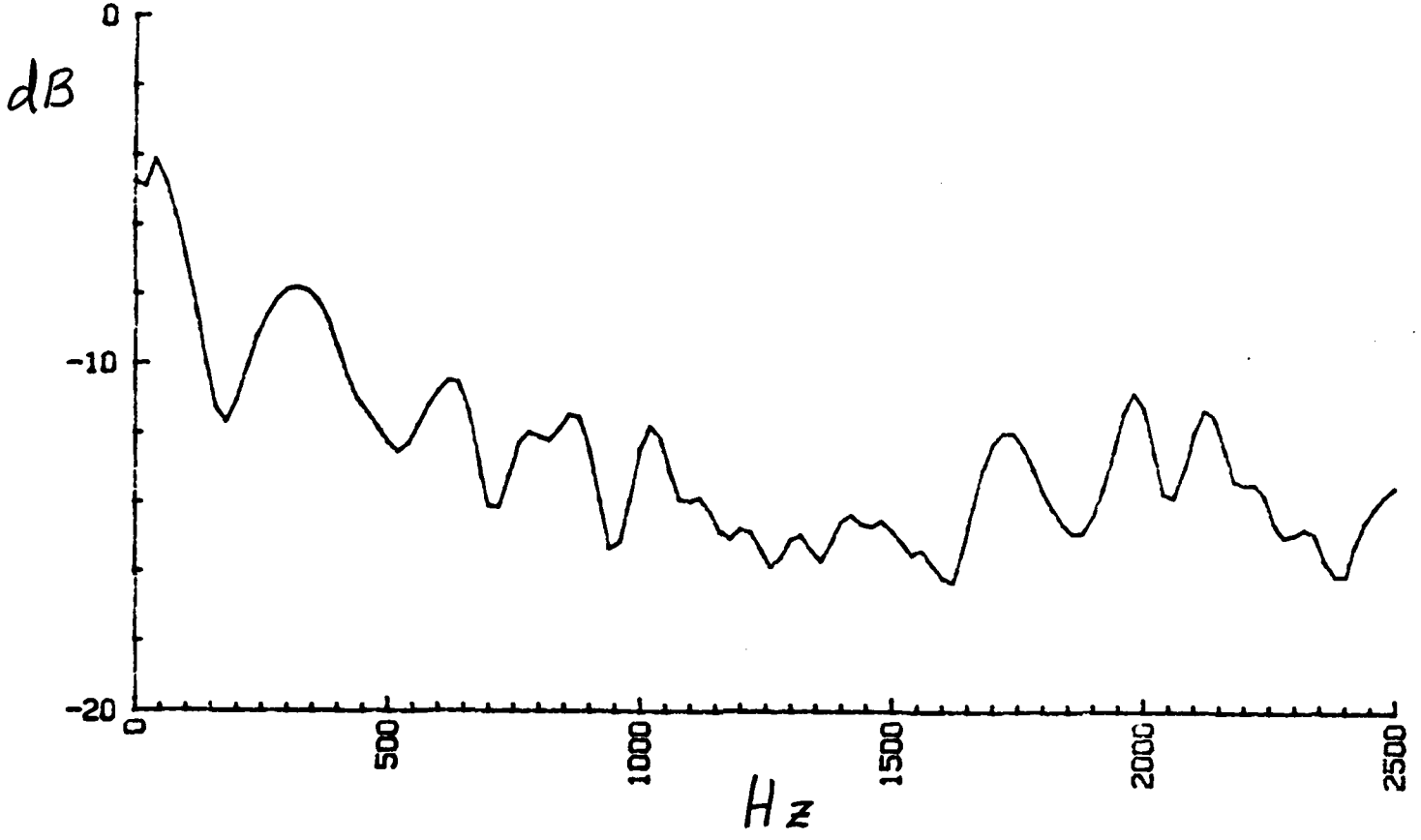

Fig 11a

CROSS SPECTRUM PHASE
256 ave, X=0 mm, Y=8.3 mm, VEL=12m/s

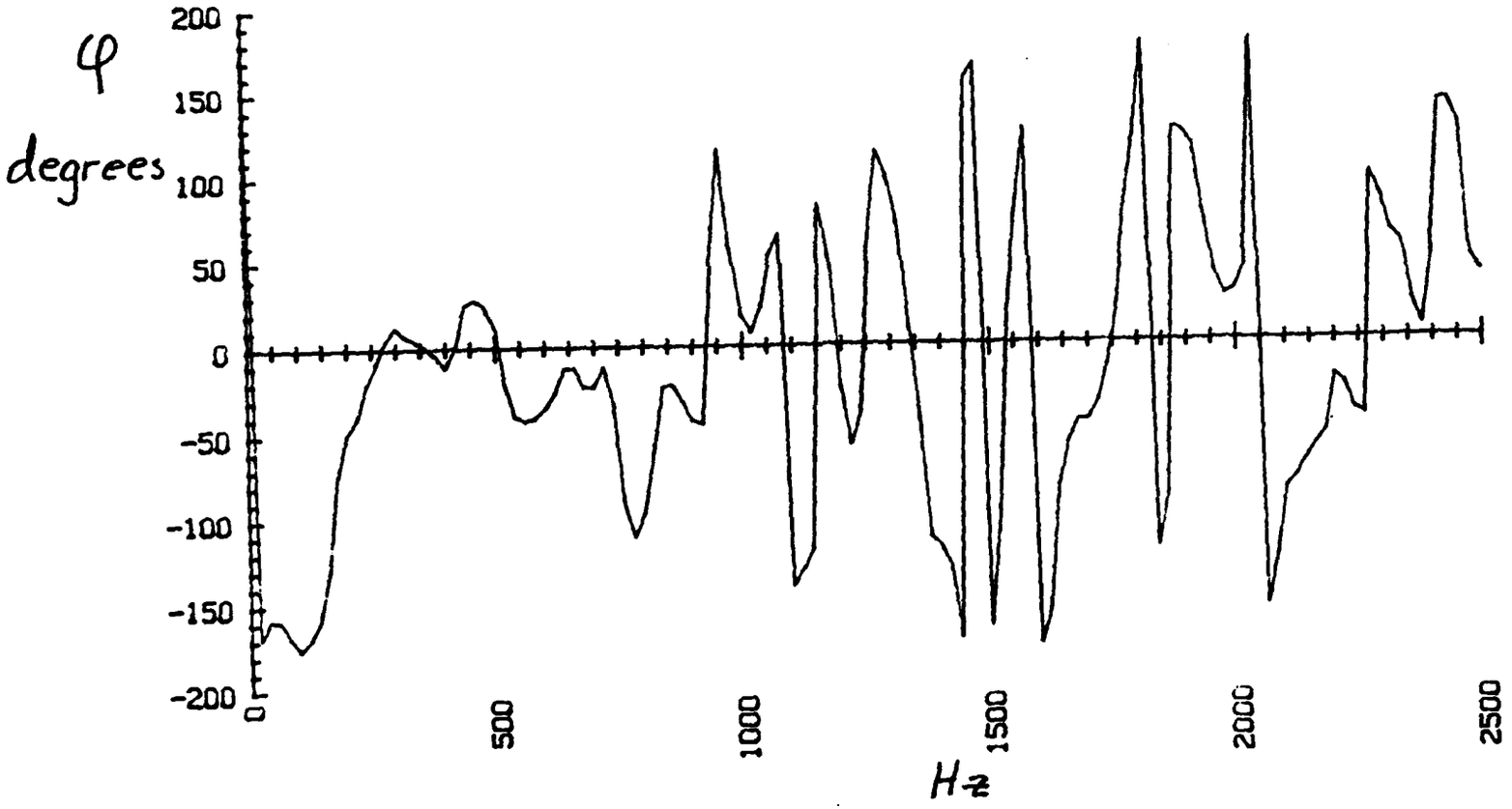

Fig 11b

NORMALIZED CROSS SPECTRUM LEVEL (dB)

256 ave. X =5.3 mm, Y=0 mm, VEL=12 m/s

Fig 12a

CROSS SPECTRUM PHASE
256 ave, X=5.3 mm, Y=0, VEL=12m/s

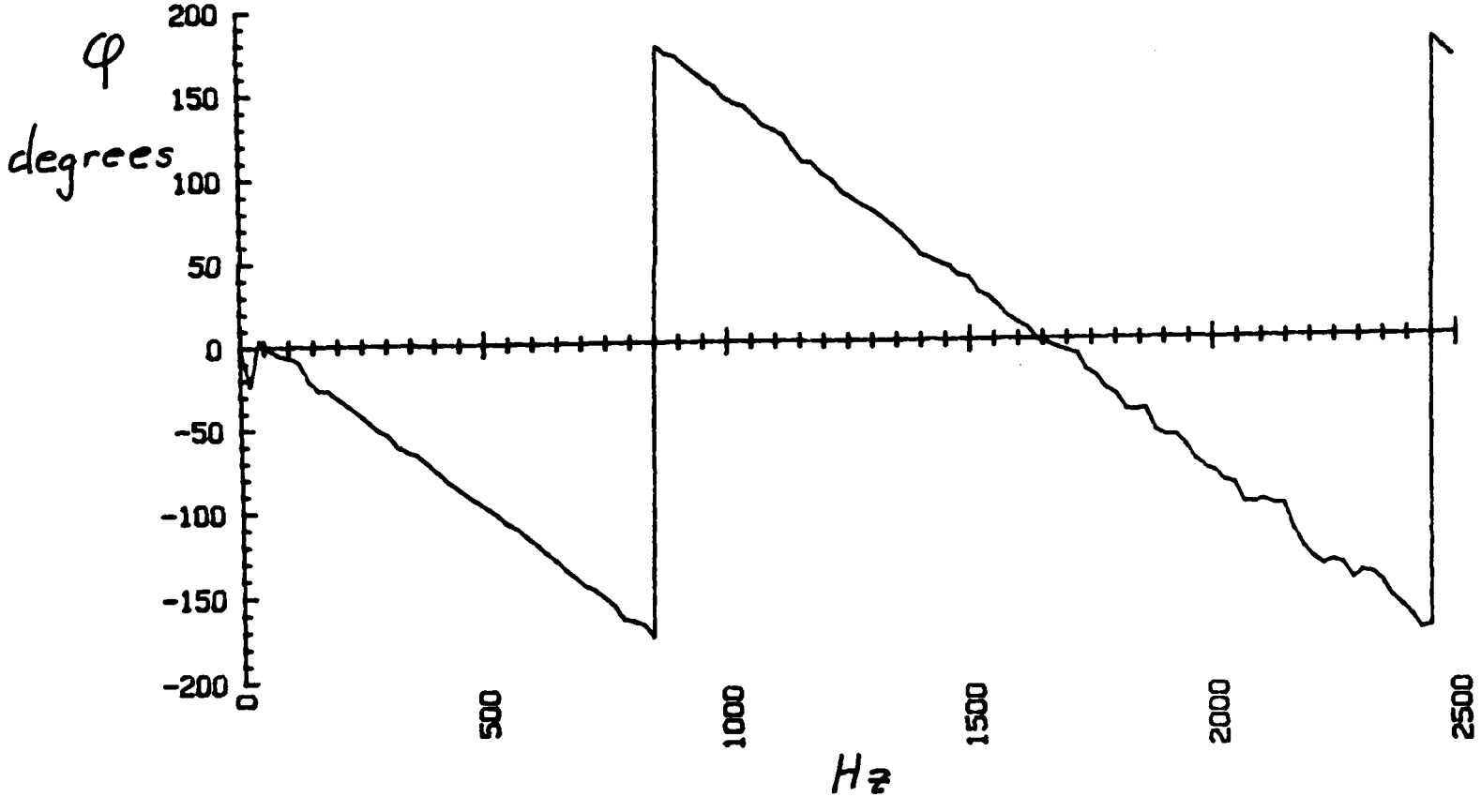

Fig 12b

NORMALIZED CROSS SPECTRUM LEVEL (dB)

256 ave, X =5.2 mm, Y=4 mm, VEL=12 m/s

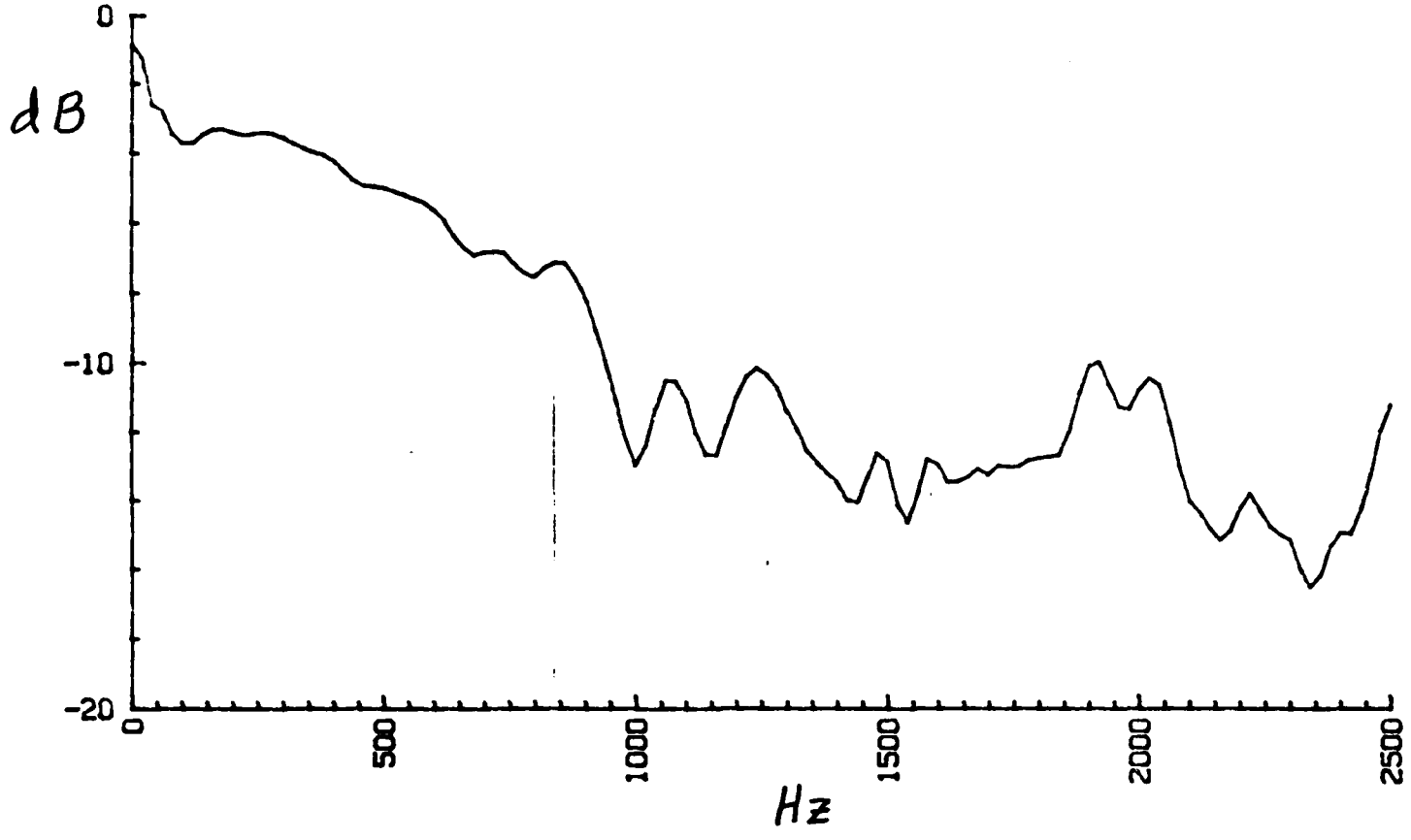

Fig 13a

CROSS SPECTRUM PHASE
256 ave, X=5.2 mm, Y=4 mm, VEL=12m/s

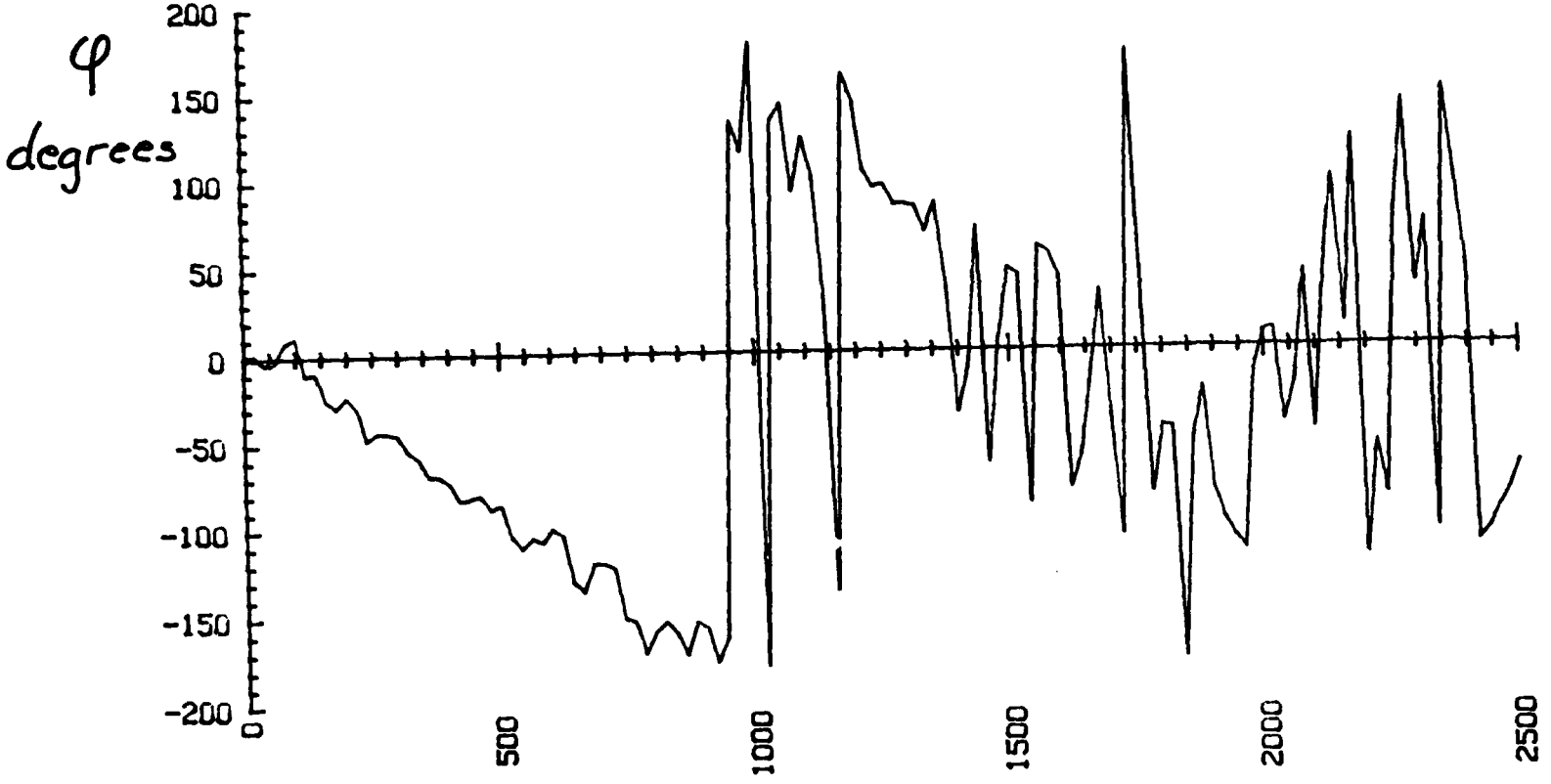

Fig 13 b

NORMALIZED CROSS SPECTRUM LEVEL (dB)

256 ave. X =5.2 mm, Y=8.2 mm, VEL=12 m/s

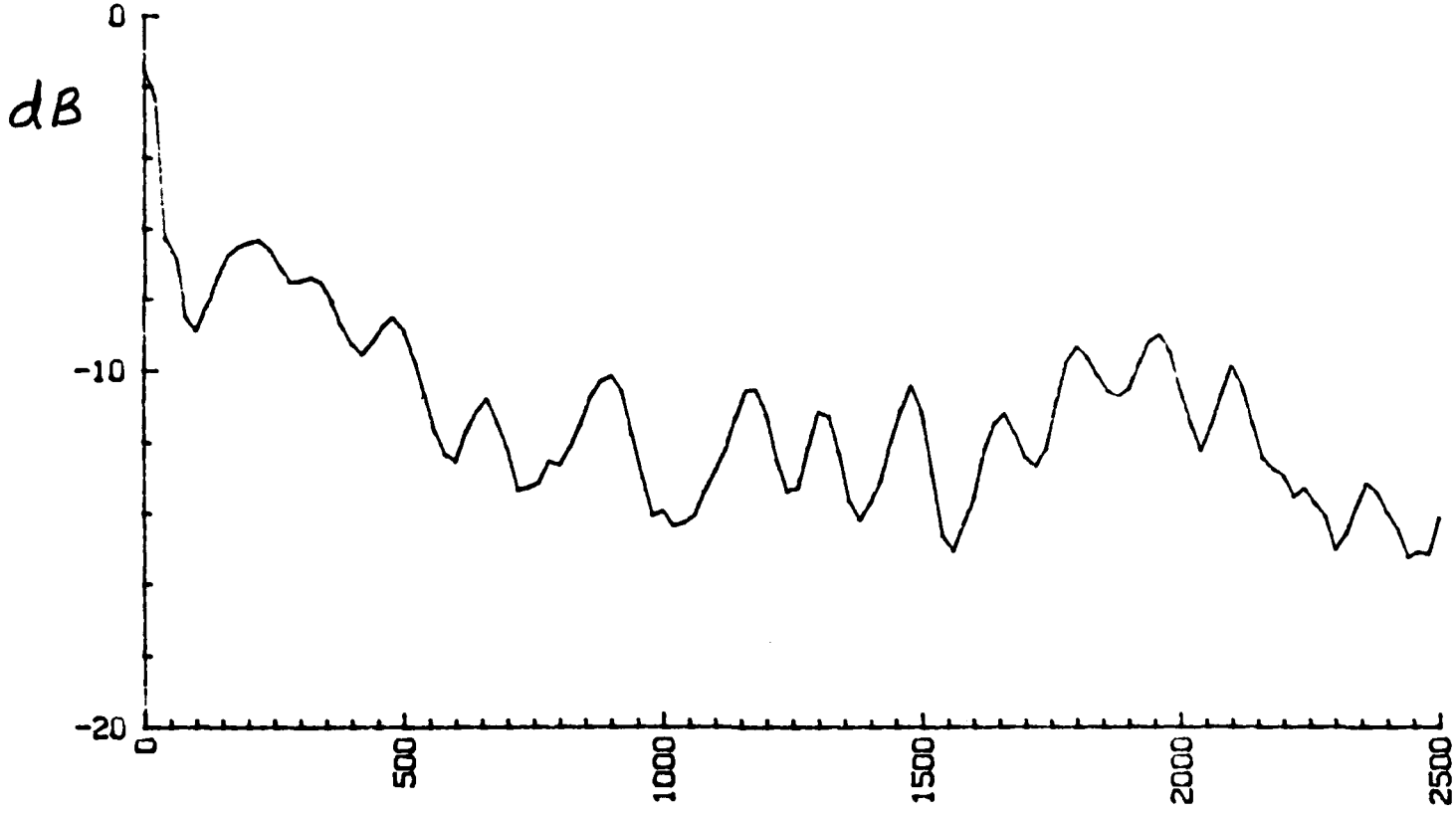

Fig 14a

CROSS SPECTRUM PHASE
256 ave, X=5.2 mm, Y=8.2mm, VEL=12m/s

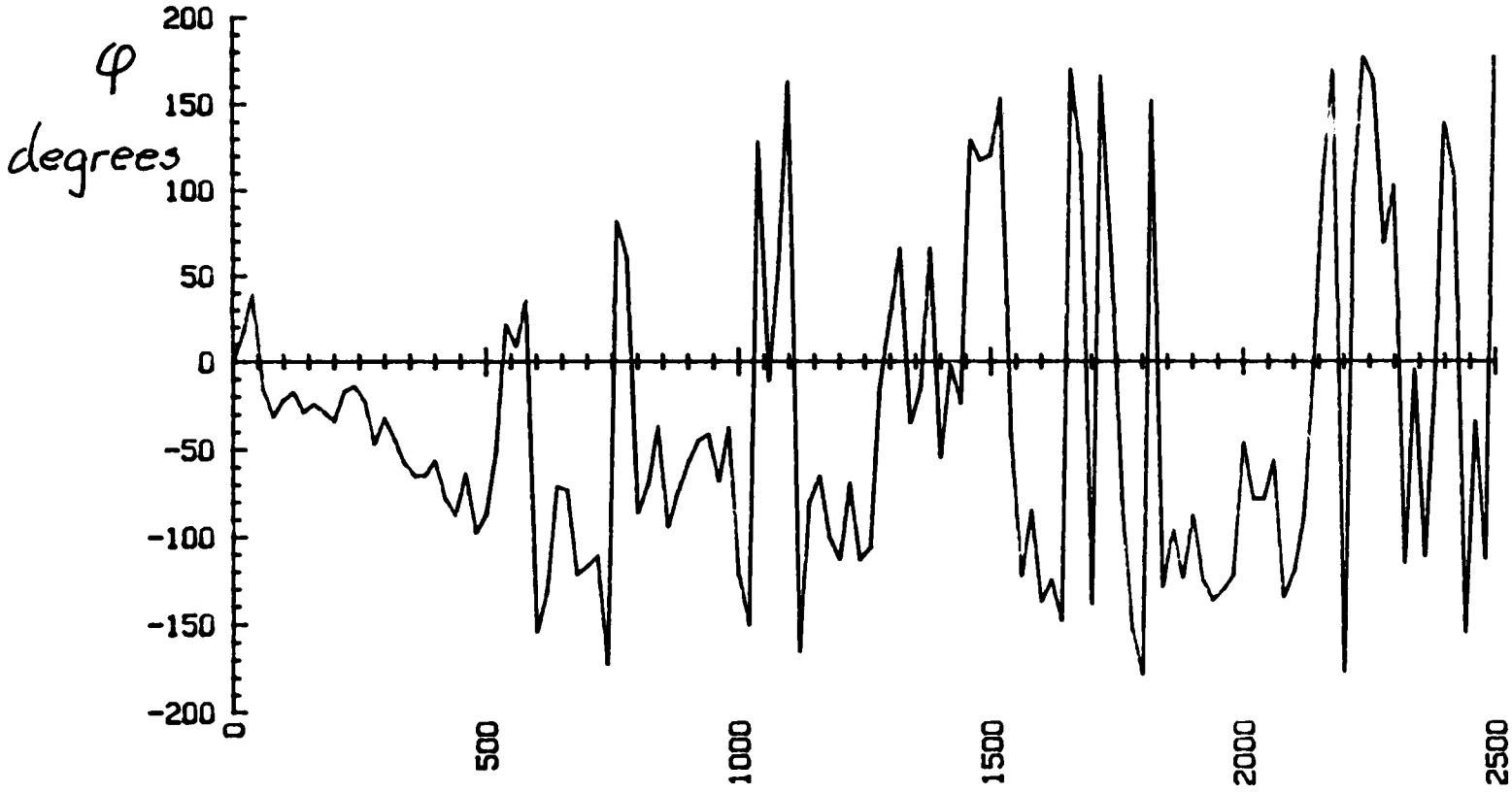

Fig 14b

NORMALIZED CROSS SPECTRUM LEVEL (dB)

256 ave, X =24.9 mm, Y=0 mm, VEL=12 m/s

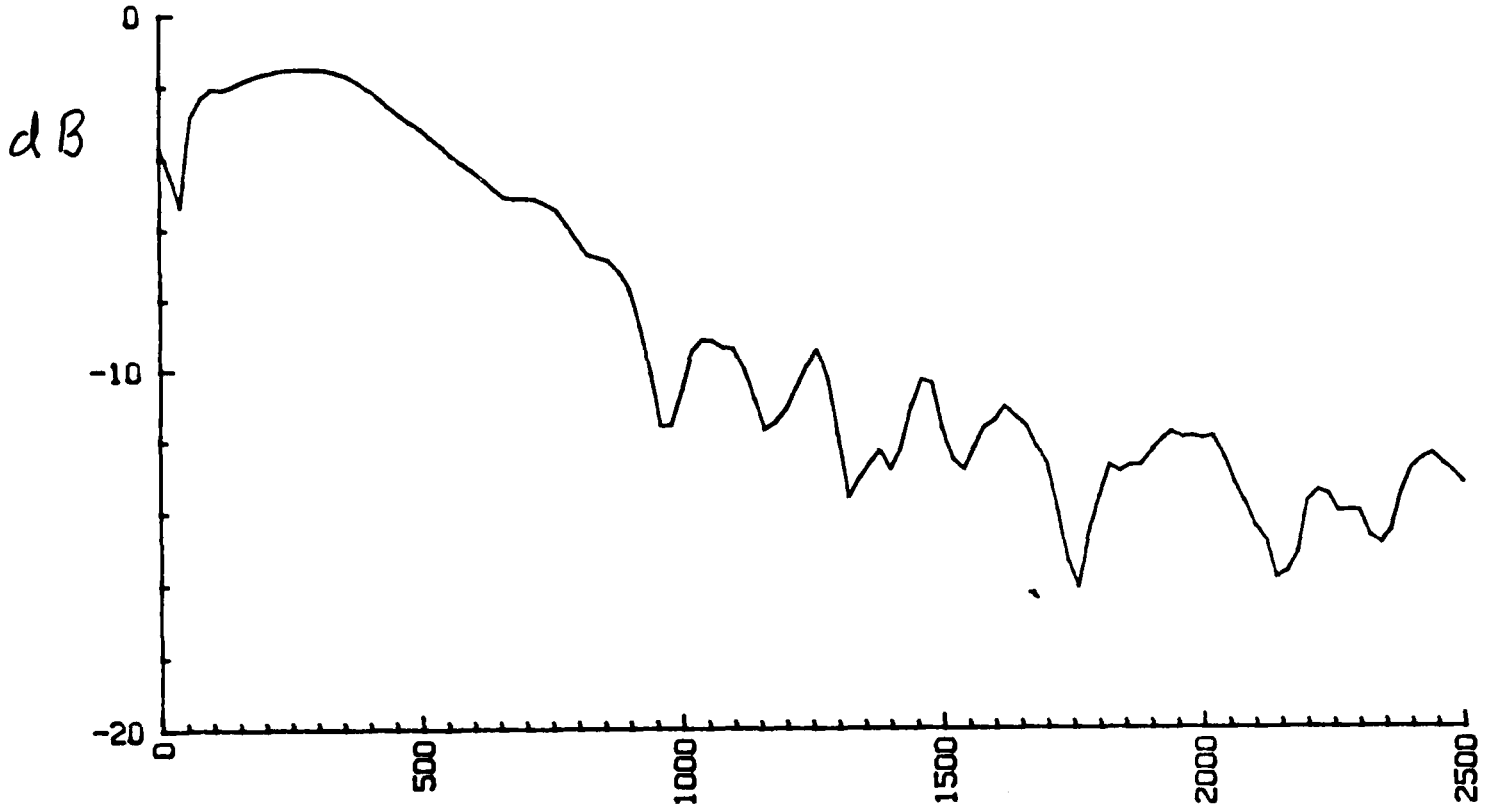

Fig 15a

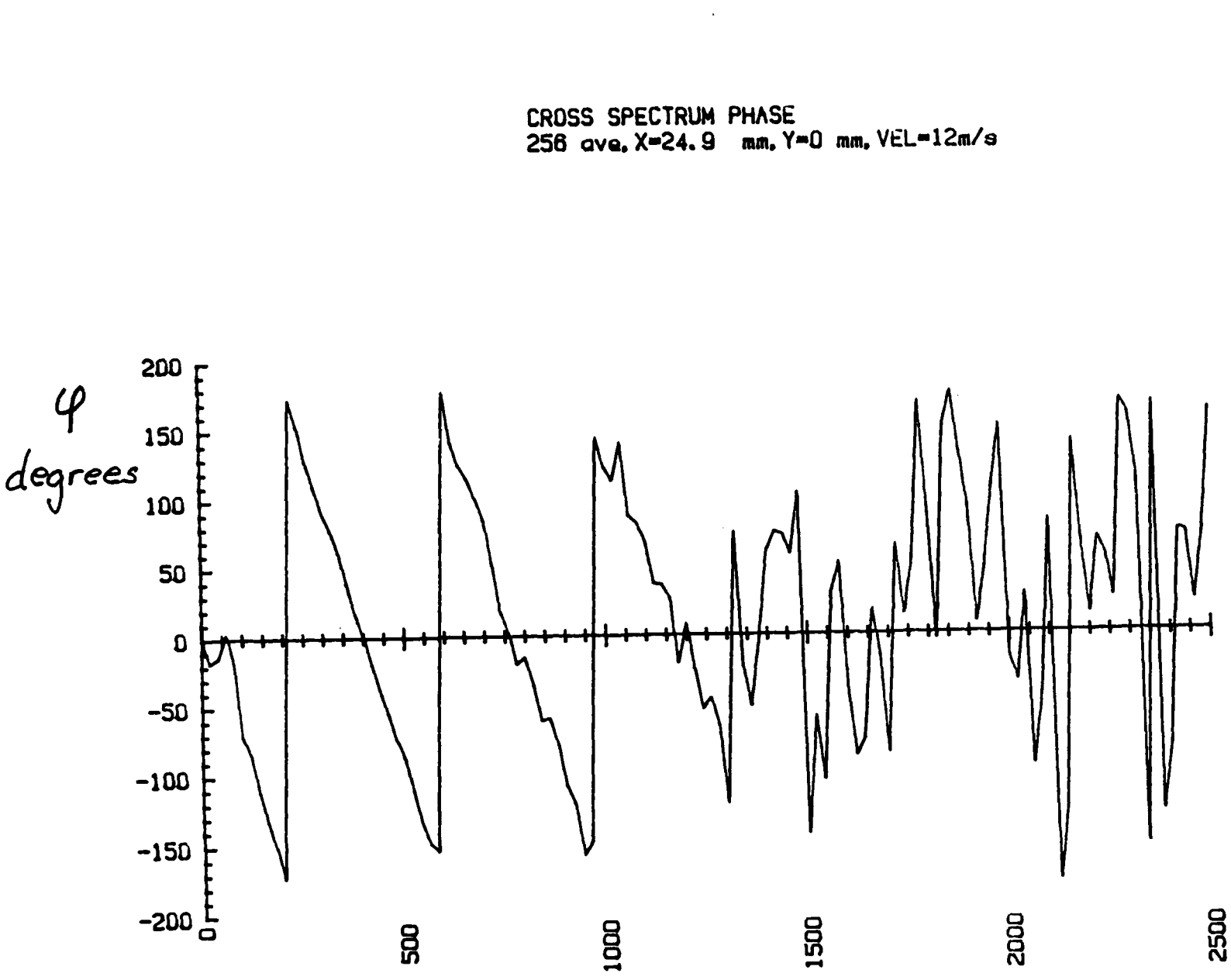
CROSS SPECTRUM PHASE
256 ave. X=24.9 mm, Y=0 mm, VEL=12m/s
φ
degrees
200
150
100
50
0
-50
-100
-150
-200
0
500
1000
1500
2000
2500

Fig 15b

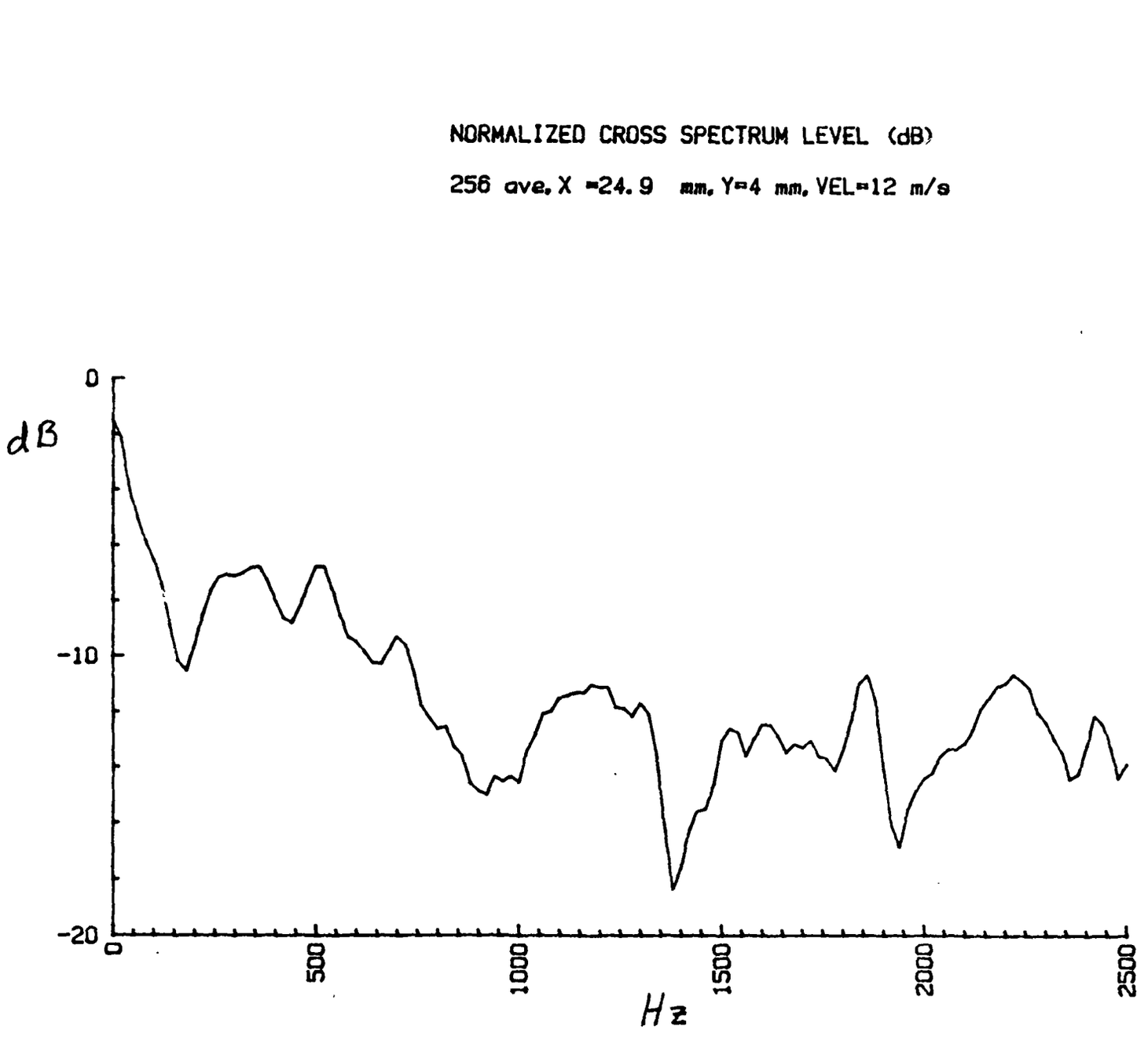
NORMALIZED CROSS SPECTRUM LEVEL (dB)
256 ave, X =24.9 mm, Y=4 mm, VEL=12 m/s
dB
0
-10
-20
0
500
1000
1500
2000
2500
Hz

Fig 16a

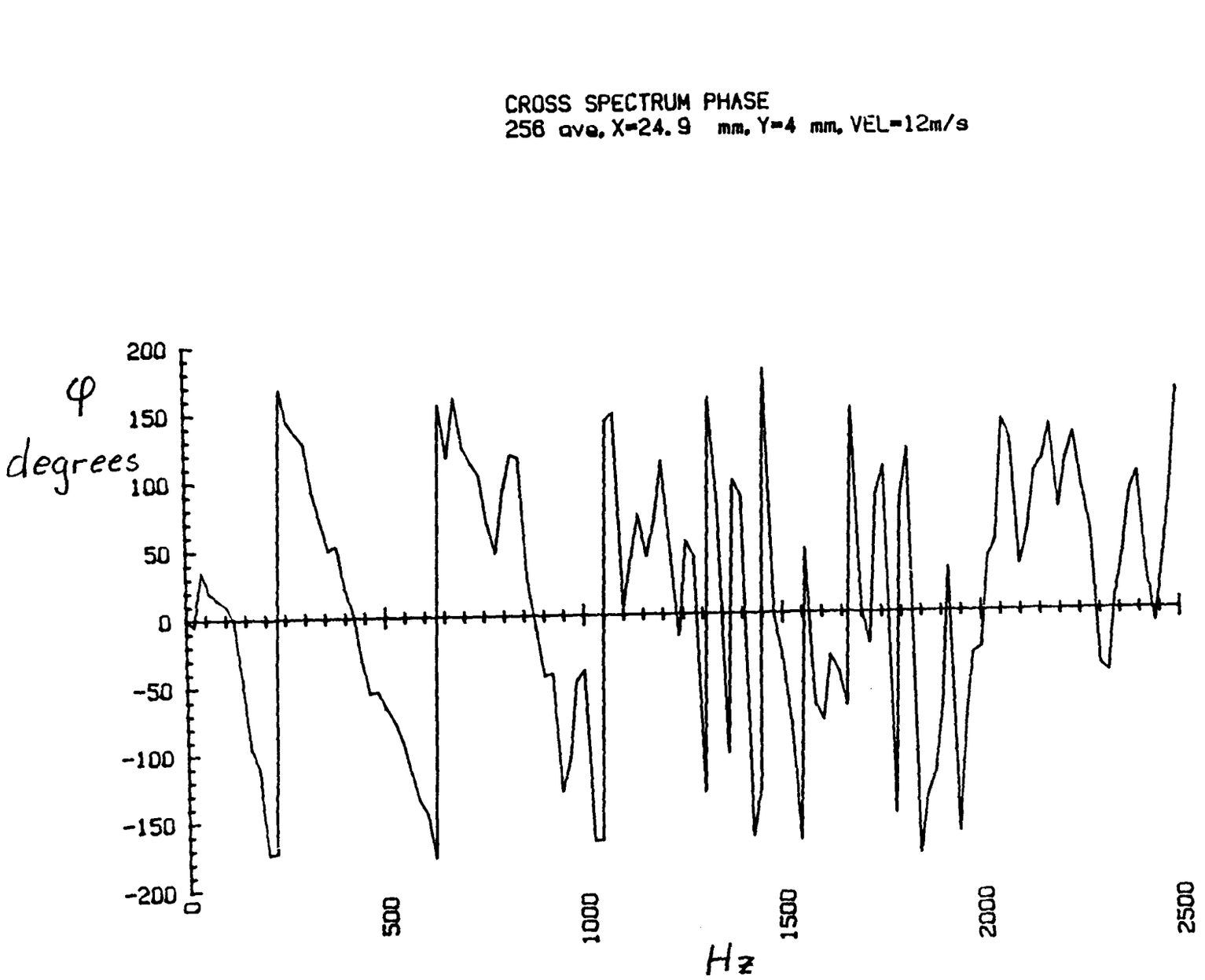
CROSS SPECTRUM PHASE
256 ave, X=24.9 mm, Y=4 mm, VEL=12m/s
φ
degrees
200
150
100
50
0
-50
-100
-150
-200
0
500
1000
1500
2000
2500
Hz

Fig 16b

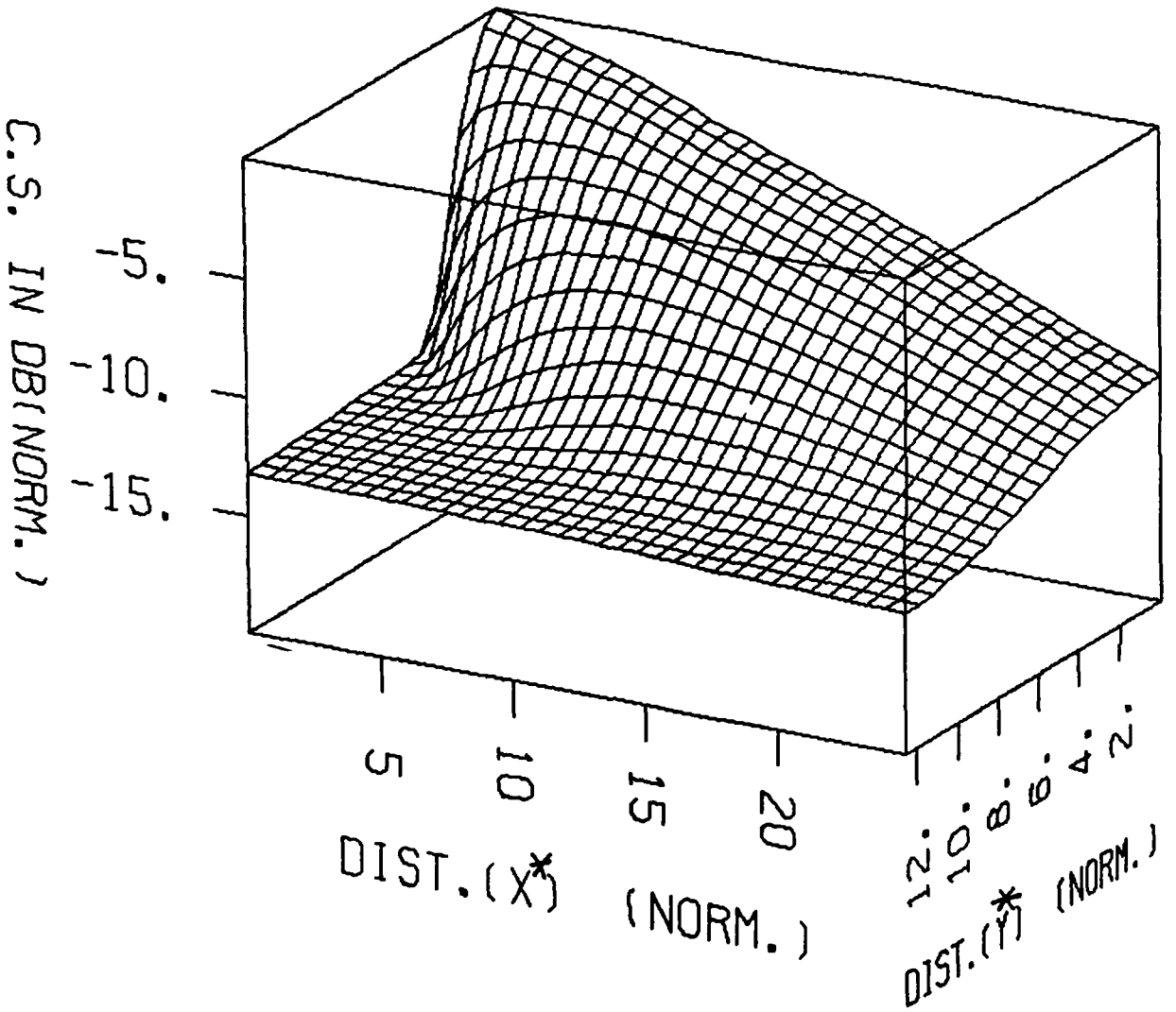

Fig 23

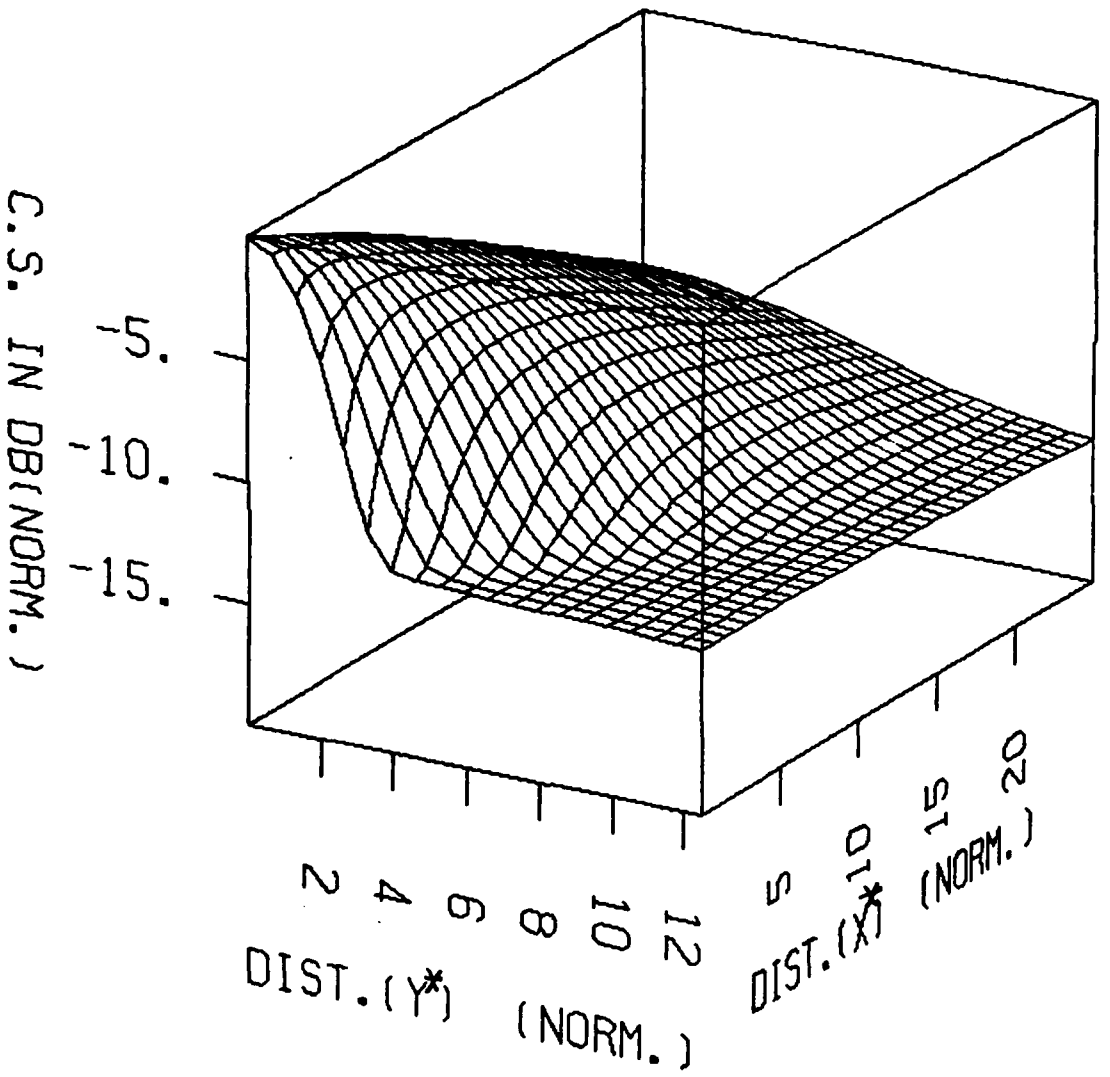

Fig 22

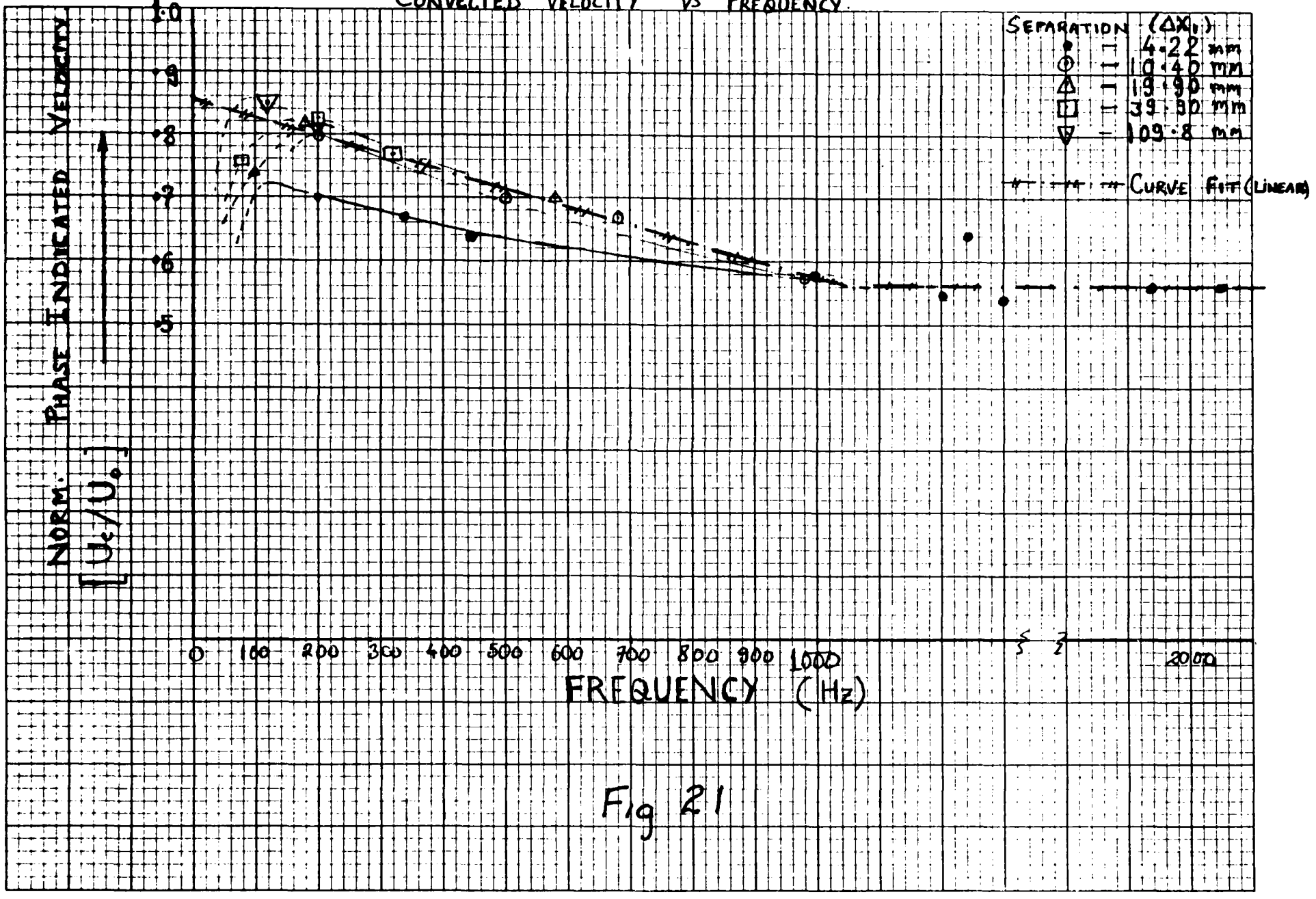
CONVECTED VELOCITY VS FREQUENCY.
SEPARATION (ΔX1)
4·22 mm
10·40 mm
19·90 mm
39·80 mm
109·8 mm
CURVE FIT (LINEAR)
NORM. PHASE INDICATED VELOCITY [Uc/Uo]
1·0
·9
·8
·7
·6
·5
0
100
200
300
400
500
600
700
800
900
1000
2000
FREQUENCY (Hz)

Fig 21

NORMALIZED CROSS SPECTRUM LEVEL (dB)

256 ave, X =110.0 mm, Y=8 mm, VEL=12 m/s

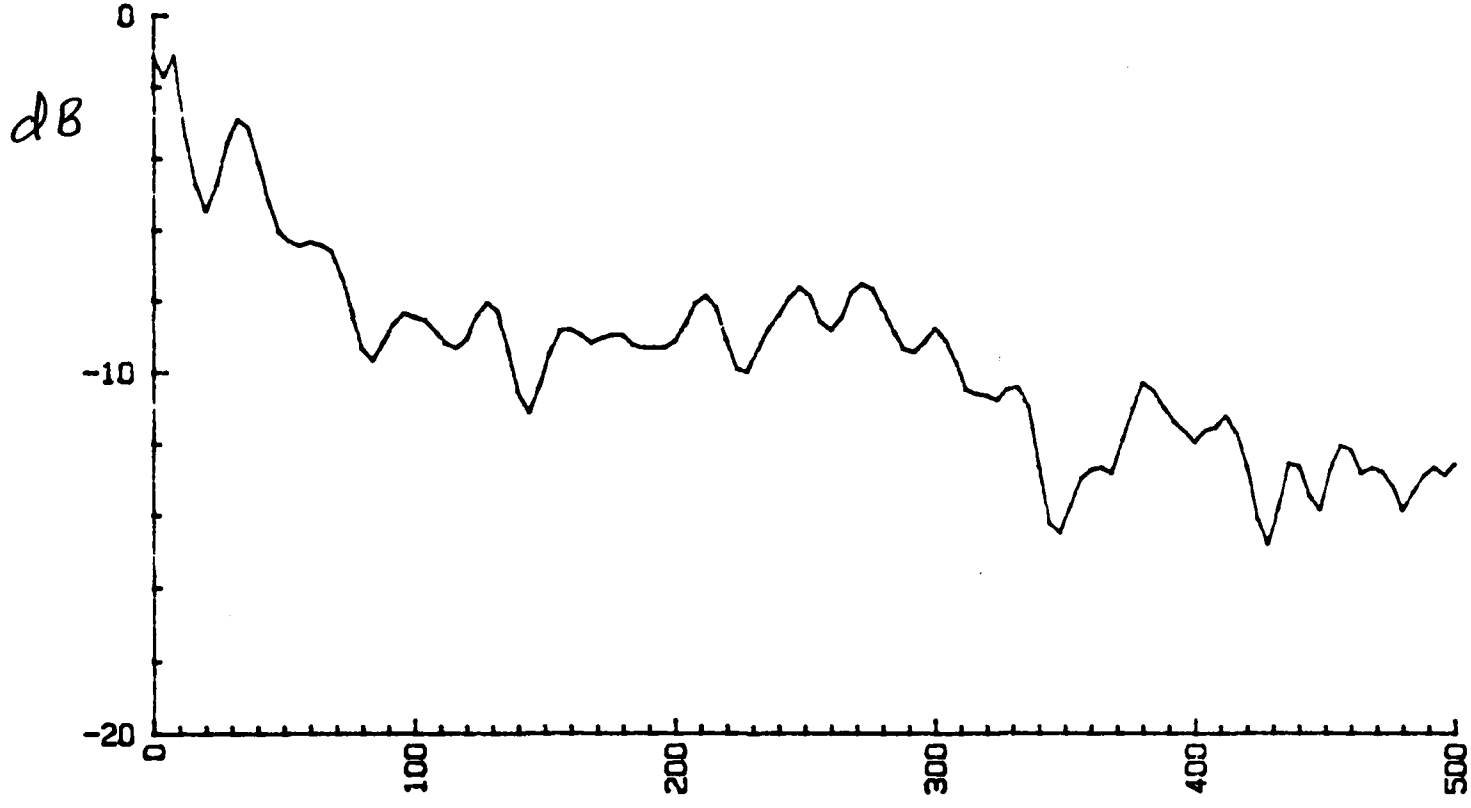

Fig20c

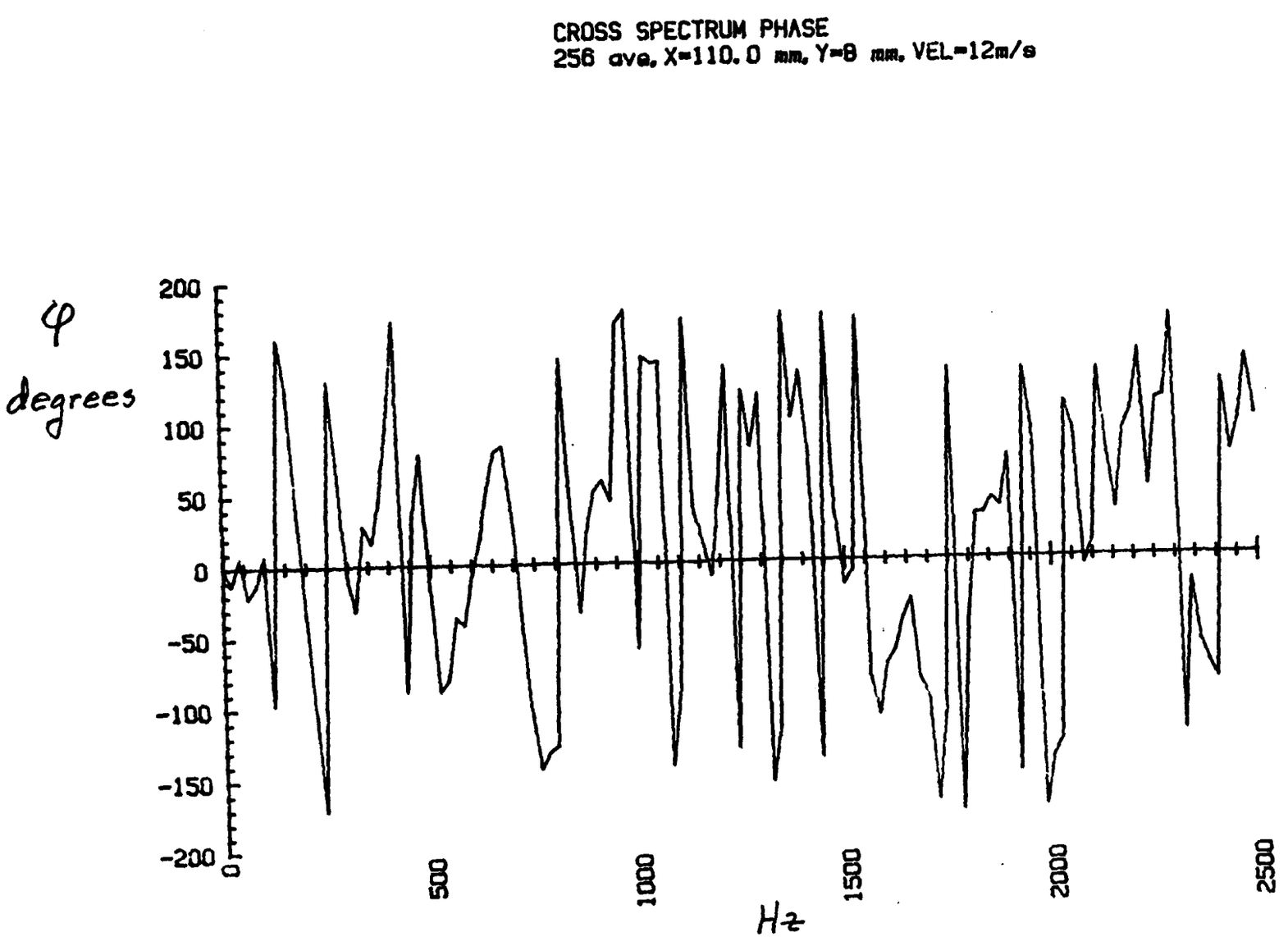
CROSS SPECTRUM PHASE
256 ave, X=110.0 mm, Y=8 mm, VEL=12m/s
φ
degrees
200
150
100
50
0
-50
-100
-150
-200
0
500
1000
1500
2000
2500
Hz

Fig 20b

NORMALIZED CROSS SPECTRUM LEVEL (dB)

256 ave, X =110.0 mm, Y=8 mm, VEL=12 m/s

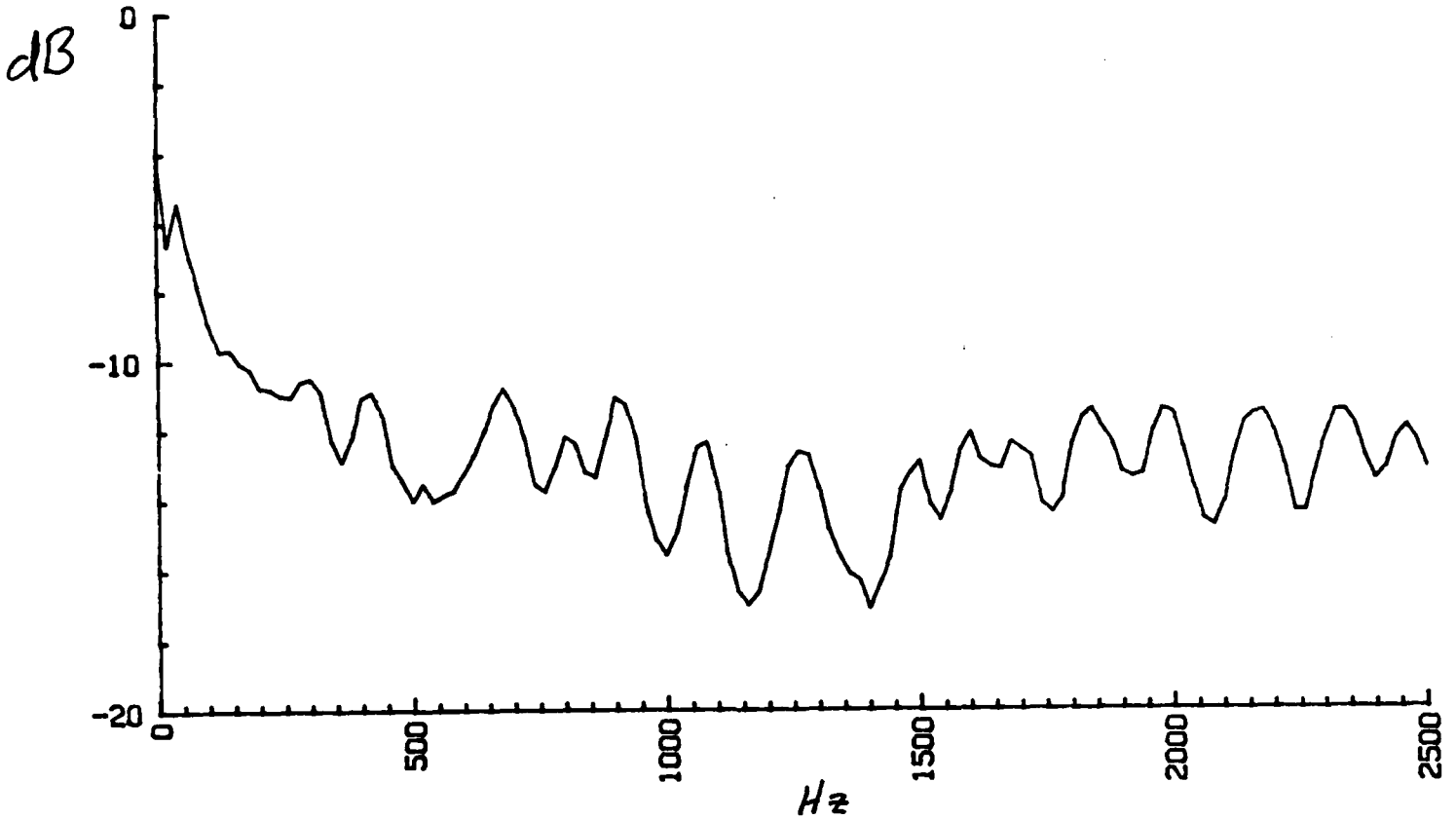

Fig 20a

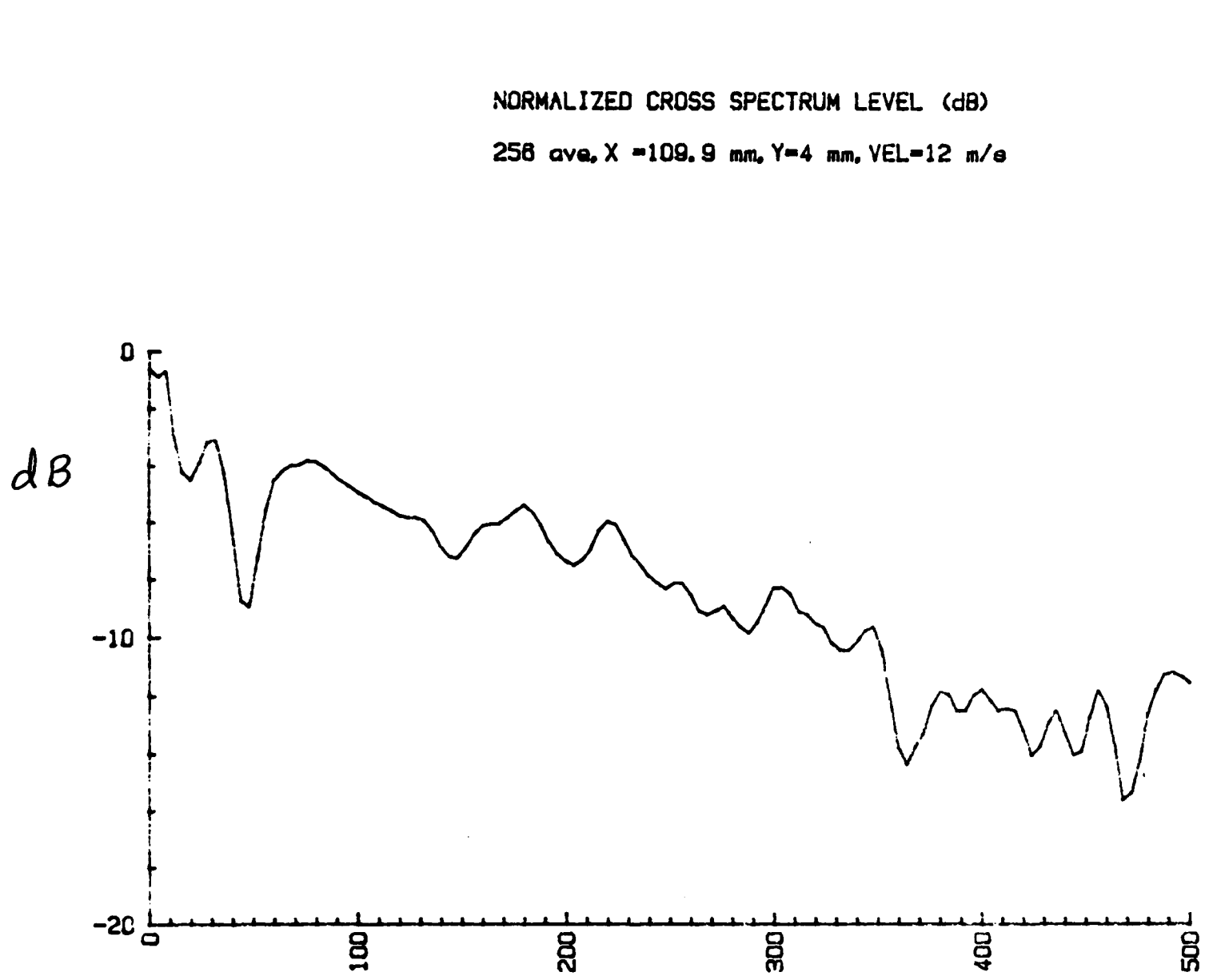
NORMALIZED CROSS SPECTRUM LEVEL (dB)
256 ave, X =109.9 mm, Y=4 mm, VEL=12 m/s
dB
0
-10
-20
0
100
200
300
400
500

Fig 19c

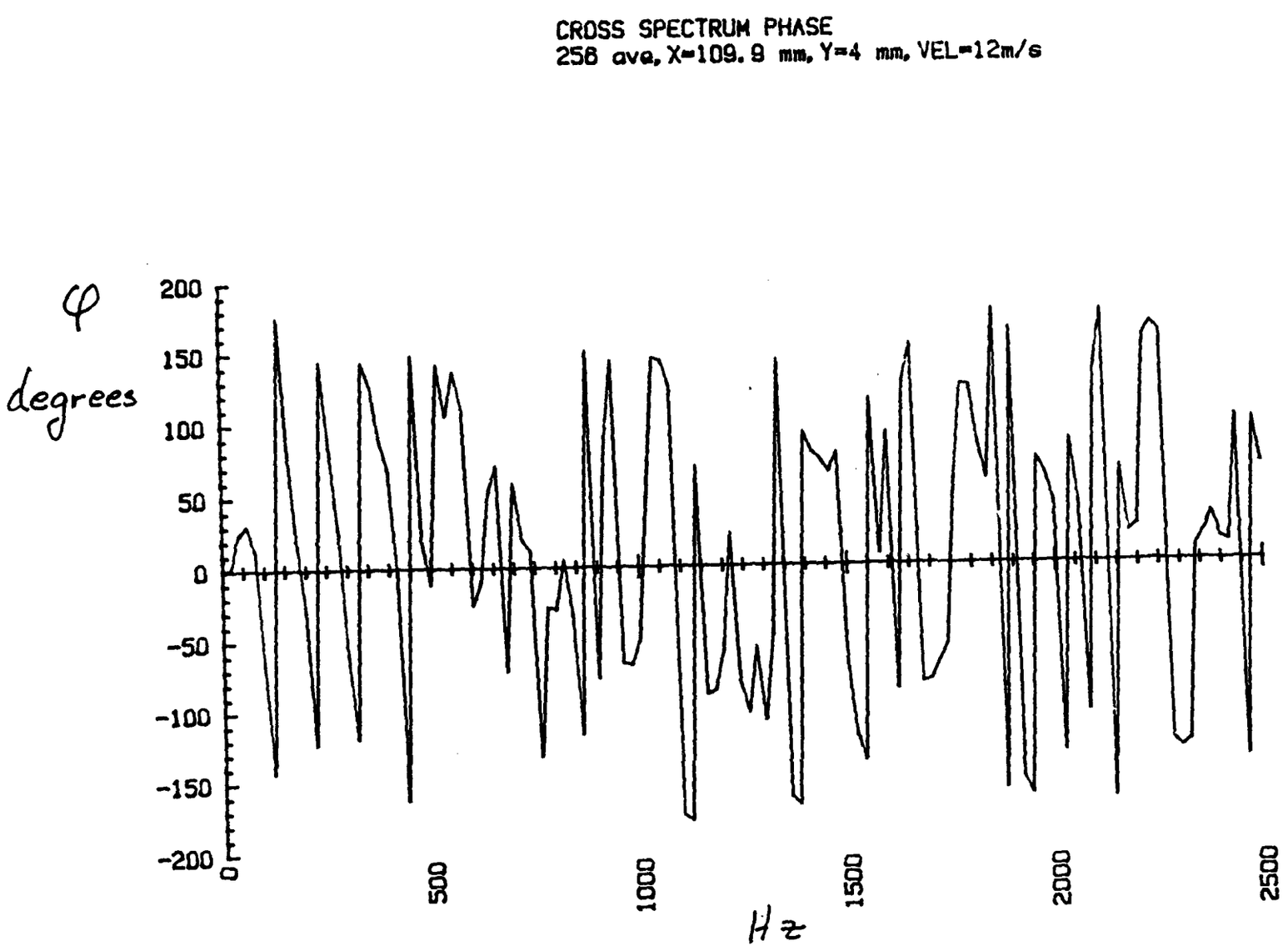
CROSS SPECTRUM PHASE
256 ave, X=109.9 mm, Y=4 mm, VEL=12m/s
φ
degrees
200
150
100
50
0
-50
-100
-150
-200
0
500
1000
1500
2000
2500
Hz

Fig 19b

NORMALIZED CROSS SPECTRUM LEVEL (dB)

256 ave, X =109.9 mm, Y=4 mm, VEL=12 m/s

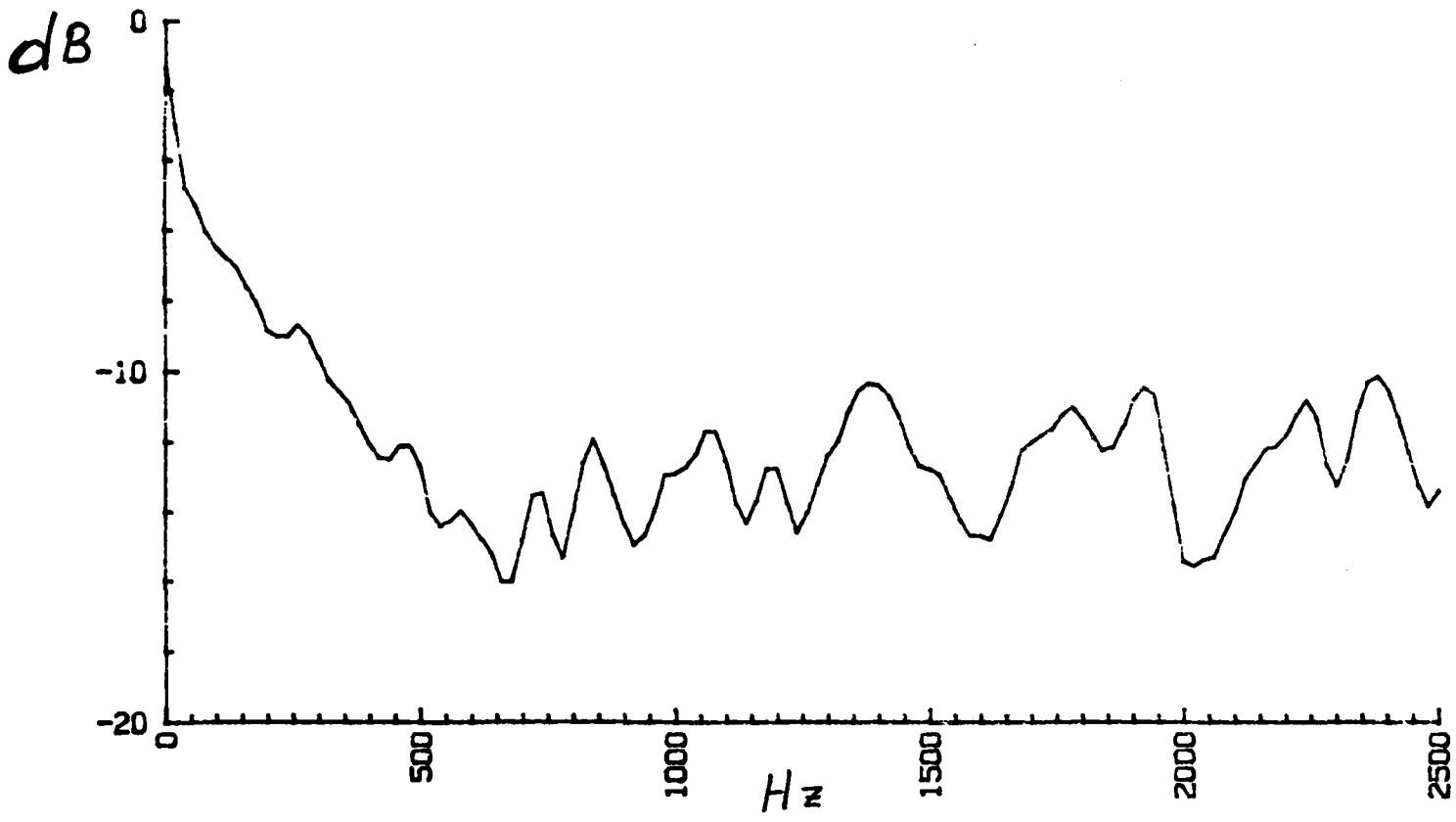

Fig 19a

NORMALIZED CROSS SPECTRUM LEVEL (dB)

256 ave, X =109.8 mm, Y=0 mm, VEL=12 m/s

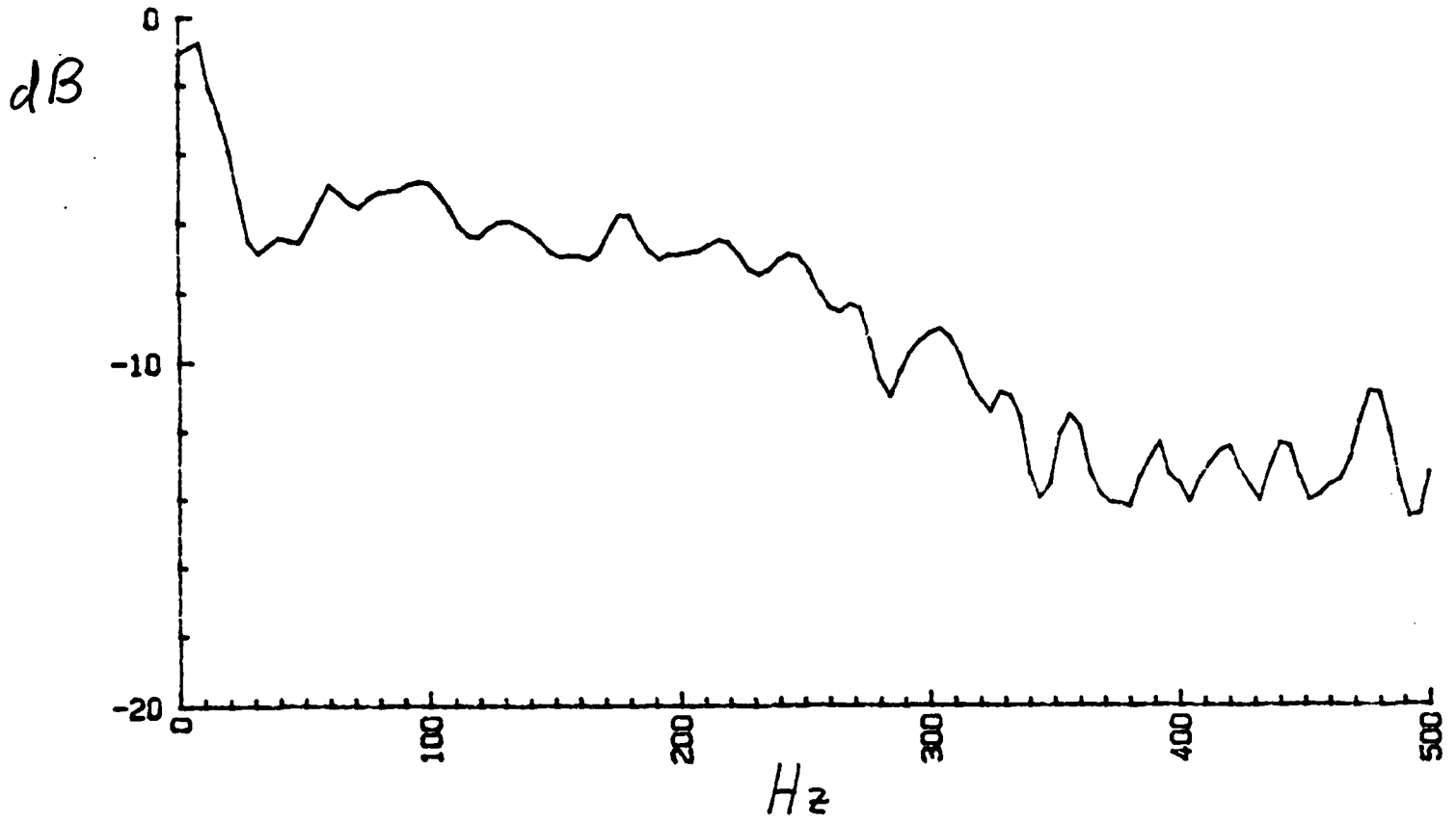

Fig 18c

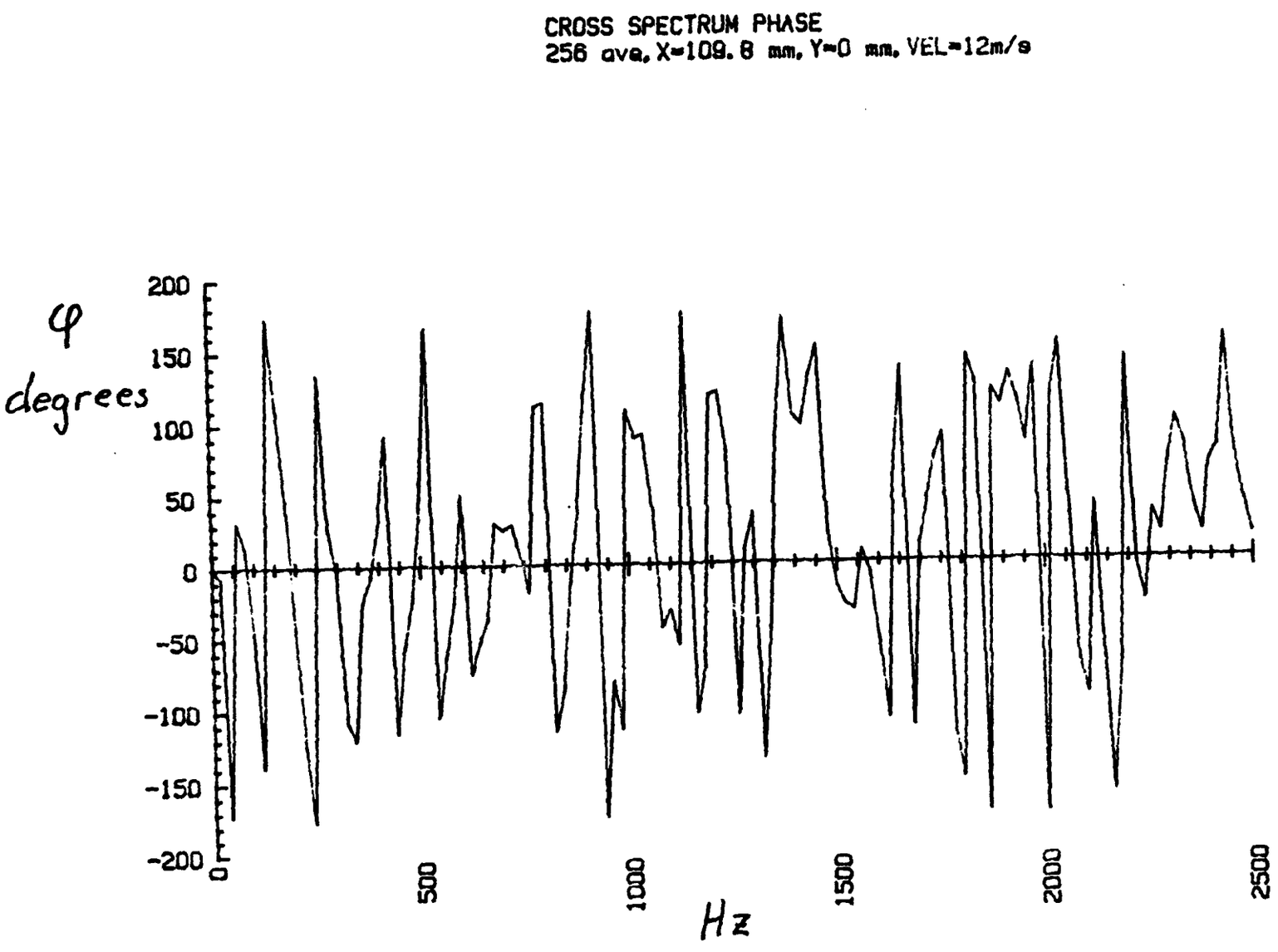
CROSS SPECTRUM PHASE
256 ave, X=109.8 mm, Y=0 mm, VEL=12m/s
φ
degrees
200
150
100
50
0
-50
-100
-150
-200
0
500
1000
1500
2000
2500
Hz

Fig 18b

NORMALIZED CROSS SPECTRUM LEVEL (dB)

256 ave, X =109.8 mm, Y=0 mm, VEL=12 m/s

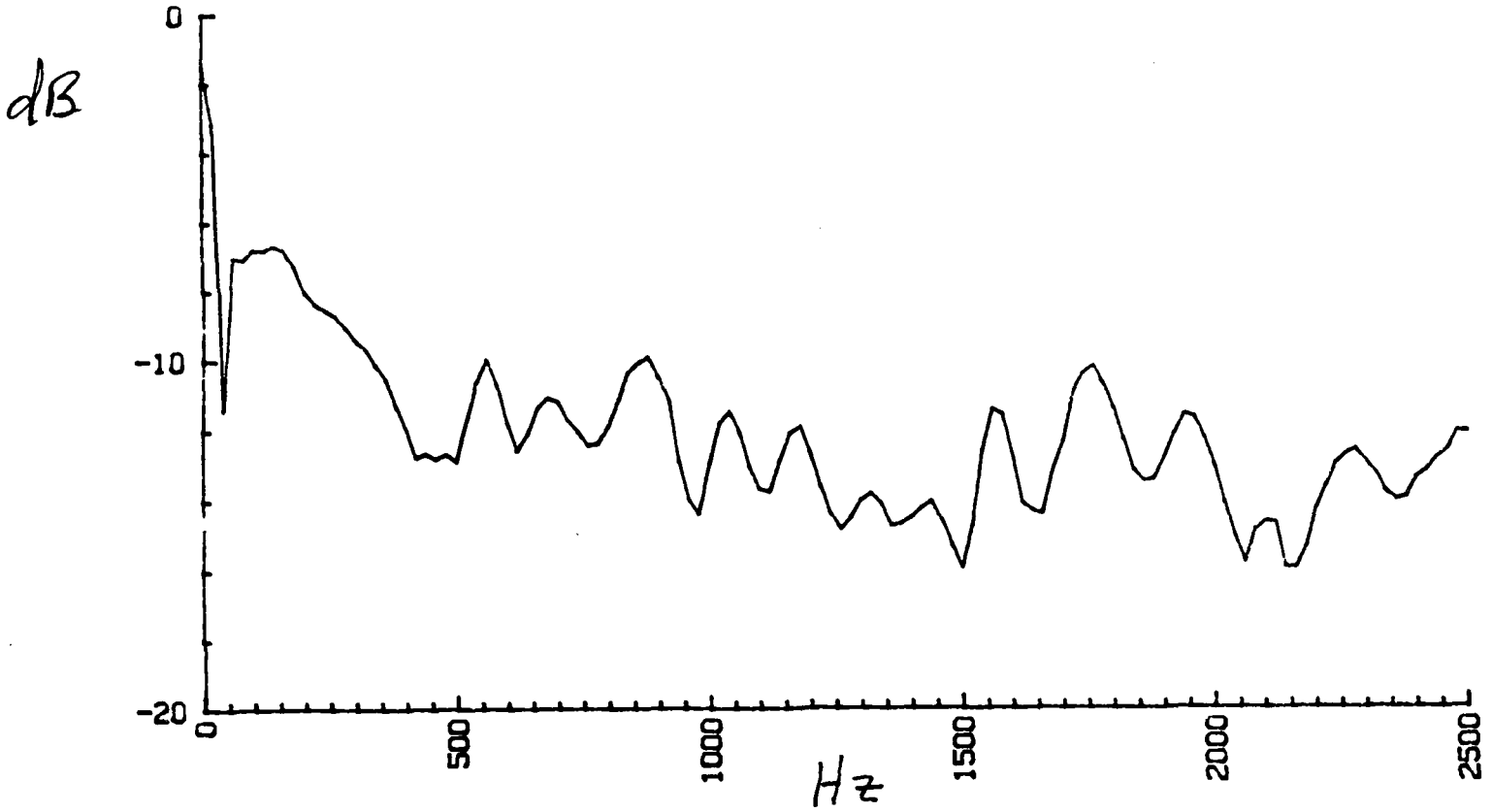

Fig 18a

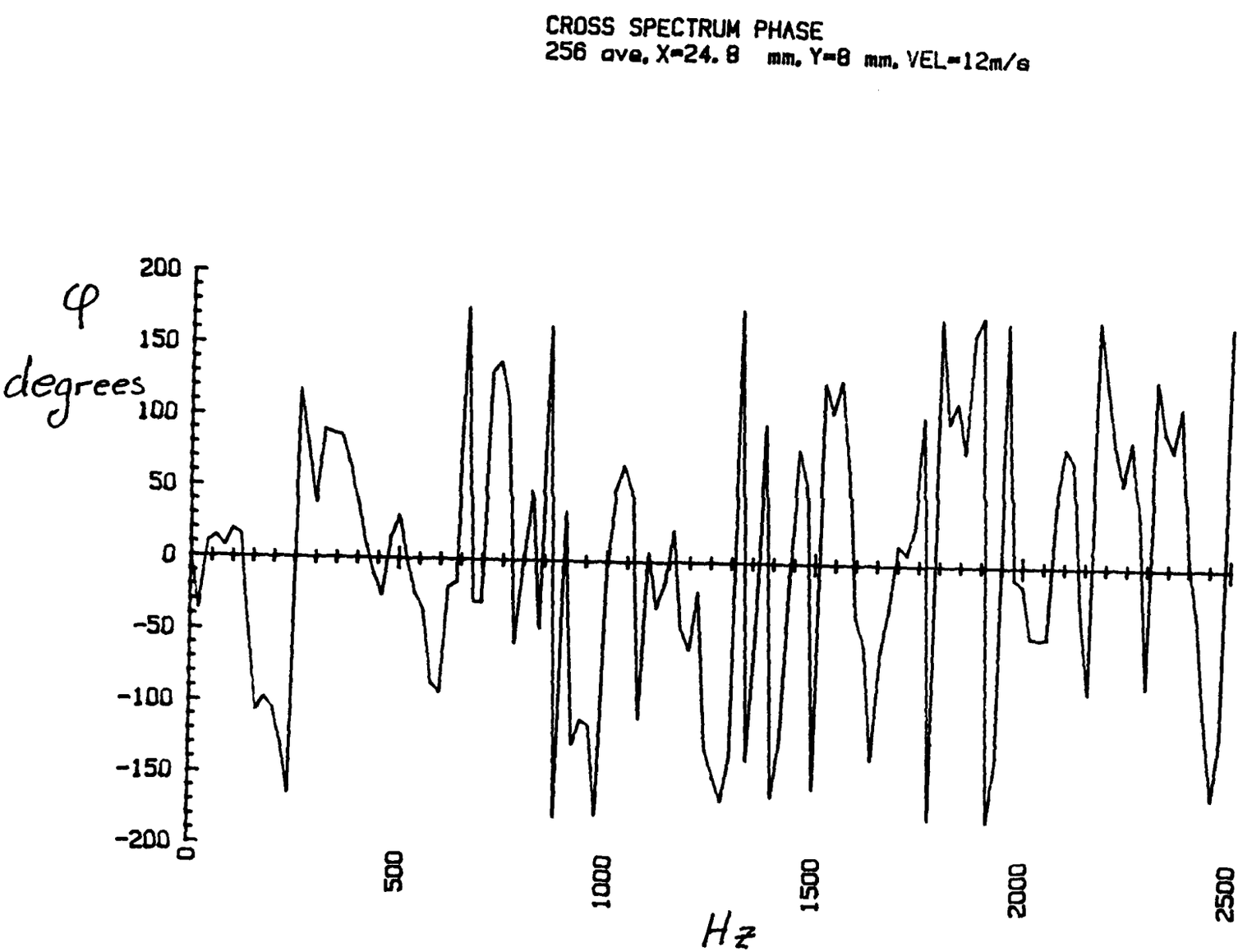
CROSS SPECTRUM PHASE
256 ave. X=24.8 mm. Y=8 mm. VEL=12m/s
φ
degrees
200
150
100
50
0
-50
-100
-150
-200
0
500
1000
1500
2000
2500
Hz

Fig 17b


NORMALIZED CROSS SPECTRUM LEVEL (dB)
256 ave, X =24.8 mm, Y=8 mm, VEL=12 m/s
dB
0
-10
-20
0
500
1000
1500
2000
2500
Hz

Fig 17a

NORM. C.S. vs NORM. AXIAL SEP.

.... X=5 mm
**** X=10mm
++++ X=30mm

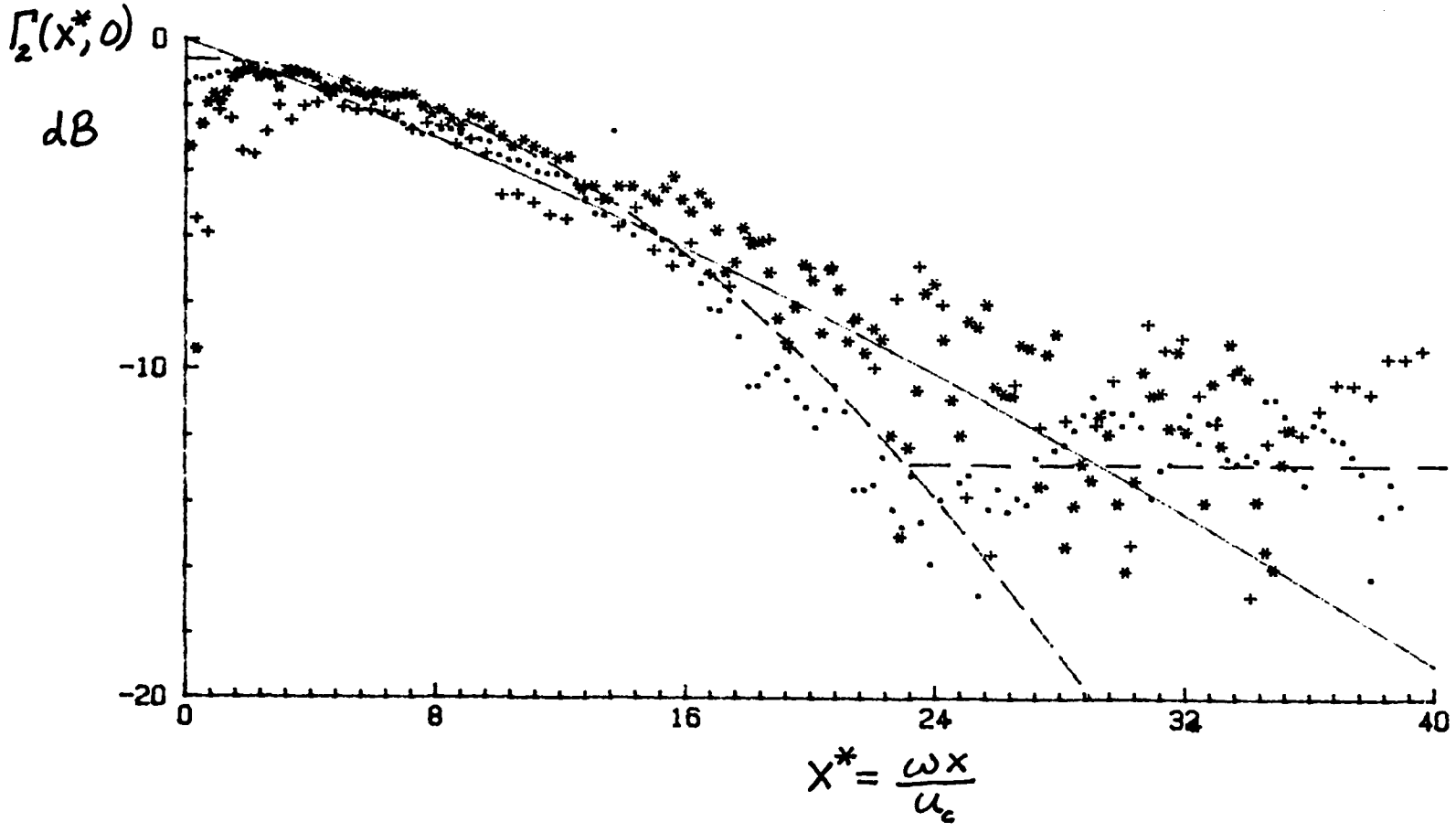

Fig 24

END

FILMED

8-85

DTIC